



**UiT** The Arctic University of Norway

Department of Medical Biology, Faculty of Health Sciences

**Virtual screening and in vitro evaluation of putative positive allosteric modulators of the GABAB receptor**

.

Ibrahim Toure Issifou

Master thesis in Pharmacy, FAR-3911, May 2020

## Table of Contents

Abbreviations .....	3
Abstract .....	7
1 Introduction .....	8
1.1 The Nervous System .....	8
1.2 Synaptic transmission.....	10
1.3 Cell surface receptors .....	11
1.4 G-protein coupled receptors .....	12
1.1.1 Activation of the GPCR .....	13
1.1.2 Beta-arrestin signaling pathway .....	14
1.5 Classification of the GPCR .....	15
1.6 Class C GPCR .....	16
1.7 Allosteric modulation .....	16
1.8 Metabotropic glutamate receptors (mGluRs):.....	17
1.9 GABAergic system.....	18
1.10 Allosteric modulation of the GABA <sub>B</sub> receptor.....	20
1.11 Molecular modelling .....	22
1.1.3 Molecular and quantum mechanics.....	22
1.1.4 Force fields .....	23
1.1.5 Energy minimization .....	23
1.1.6 Homology modelling.....	23
1.12 Drug design .....	26
1.1.7 Virtual Screening (VS):.....	28
2 Aim.....	30
3 Methods.....	31
3.1.1 Software packages .....	31
3.1.2 Databases.....	32

3.1.3	Homology modelling.....	33
3.1.4	Ligand preparation .....	35
3.1.5	Receptor setup .....	35
3.1.6	Docking, scoring and model selection .....	35
3.1.7	Induced fit docking.....	36
3.1.8	Virtual screening of Molport and DrugBank .....	36
3.1.9	Part II: In Vitro .....	39
4	Results .....	46
5	Discussion .....	58
6	Conclusion.....	69

## Abbreviations

<b>ADH</b>	Antidiuretic Hormone
<b>ADME</b>	Absorption Distribution Metabolism Excretion
<b>BLAST</b>	Basic Local Alignment Search Tool
<b>C-terminal</b>	Carbon - terminal
<b>CNS</b>	Central Nervous System
<b>Da</b>	Dalton
<b>DUD</b>	Databased of Useful Decoys
<b>EC</b>	Effective Concentration
<b>E<sub>Angle</sub></b>	Angle Binding Energy
<b>E<sub>Bonded</sub></b>	Bonded Energy
<b>E<sub>Dihedral</sub></b>	Torsional Energy
<b>E<sub>Elec</sub></b>	Electrostatic Energy
<b>E<sub>non-bonded</sub></b>	Non-Bonded Energy
<b>E<sub>vdw</sub></b>	Van der Waals Energy
<b>GABA</b>	$\gamma$ -aminobutyric acid
<b>GAT</b>	GABA-transporter
<b>GIRK</b>	G Protein-Coupled Inwardly-Rectifying Potassium Channel
<b>GPCR</b>	G Protein-Coupled Receptor
<b>GRK</b>	G Protein-Coupled Receptor Kinase
<b>HBA</b>	Hydrogen Binding Acceptor

<b>HBD</b>	Hydrogen Binding Donor
<b>HTVS</b>	High-Throughput Virtual Screening
<b>ICM</b>	The Internal Coordinate Mechanics
<b>IFD</b>	Induced Fit Docking
<b>LBDD</b>	Ligand Based Drug Design
<b>LBVS</b>	Ligand Based Virtual Screening
<b>MGlur</b>	Metabotropic Glutamate Receptor
<b>MM</b>	Molecular Mechanics
<b>Mw</b>	Molecular Weight
<b>NMDA</b>	N-Methyl-D-Aspartate
<b>NMR</b>	Nuclear Magnetic Resonance
<b>PDB</b>	Protein Database
<b>PSA</b>	Polar Surface Area
<b>PNS</b>	Peripheral Nervous System
<b>QM</b>	Quantum Mechanics
<b>QSAR</b>	Quantitative Structure Activity Relationship
<b>SAVES</b>	Structural Analysis and Verification Server
<b>SBDD</b>	Structure Based Drug Design
<b>SBVS</b>	Structure Based Virtual Screening
<b>SP</b>	Standard Precision
<b>(7) TM</b>	Transmembrane

**UniProtKB** The Universal Protein Resource Knowledge Based

**VGCC** Voltage Gated Calcium Channels

**VS** Virtual Screening

**XP** Extra Precision

**Å** Angstrom

## Foreword

In the name of Allah, the most Gracious and the most Merciful.

The master thesis was written at the at the Medical Pharmacology and Toxicology Research Group, Department of Medical Biology, Faculty of Health Science between August 2019 – May 2020

I would first like to start by thanking the Almighty God for giving my strength to finish this master thesis. I was able to write this master thesis with His mercy. It is said that het hat doesn't thank the people is not thankful to Allah.

Therefore, I want to start by acknowledging my supervisors Mari Gabrielsen and Imin Wushur. They have been super supporting throughout this whole period. They have also been giving me feedback that have improved my master thesis. You were always ready to help me whenever I needed help. You also guided me in the right direction. For that, I want to thank them a lot for being my supervisors – I am forever grateful.

Further, I also want to thank my project partner, Ali Hadi. It was a pleasure to work with you. We made a lot of good memories together. Without your passion and dedication, this would have not been an enjoyable journey at all. It was funny to work on this master thesis with you, even though it kicked our ass's multiple times.

I definitely want to send an extended thanks to my office mates, my brothers Luqman Ahsan and Kasi Shorsh. It has been a pleasure to get to know you. My years in Tromsø would have not been the same without you. We have been able to make a lot of memories together that I cherish, and I hope we continue this friendship forever.

Last but not least, my family. They have been supporting me through my journey. They have been there for me in my darkest times. I cherish and appreciate their support. My parents and siblings have encouraged me, and for that I want to express my gratitude to them.

Thank you from the bottom of my heart.

## **Abstract**

$\gamma$ -aminobutyric acid (GABA) is the chief inhibitory neurotransmitter of the central nervous system (CNS). GABA exhibits its function by binding to either the ionotropic GABA<sub>A</sub> receptor or the metabotropic GABA<sub>B</sub> receptor, causing a decrease in activity in the nervous system. Disruption in the GABAergic system has been associated with various neurological conditions, including Alzheimer's disease, anxiety, depressive disorders, and epilepsy.

Currently, there is only one marketed drug that work on the GABA<sub>B</sub> – receptor, on the orthosteric site to be more specific. The discovery of allosteric modulators for the G-protein coupled receptors provides a promising new strategy with potential for developing novel treatments for a variety of CNS disorders, as they allow for increased drug selectivity and potentially decreased adverse side effects.

Homology models of the GABA<sub>B</sub> receptor were built due to the lack of an experimentally solved three-dimensional structure, and they were used to screen for potentially new allosteric modulators using a combination of structure-based and ligand based virtual screening (in silico) with compounds from the Molport database and DrugBank. 16 compounds were purchased for testing – 8 from each database, and were further investigated and evaluated by experimental in vitro testing.

Our results indicate that we have four hits, two from each database (DrugBank: I-4 = Mefloquine and I-10 = Rivaroxaban, Molport: I-23 and I-24) where it seems like I-4, I-23 and I-24 acts like PAMs whereas I-10 acts like a NAM/antagonist. The compounds from DrugBank, especially Mefloquine is of interest due to its well-known adverse effect profile which may be linked to the GABAergic system. Further investigation and confirmation of activity at the GABA<sub>B</sub> receptor could potentially lead to development of novel drugs as well as important tools for studying the structure and function of the GABA<sub>B</sub> receptor. And at the same time be used to explain the side effects seen when using Mefloquine.



## 1 Introduction

The human body is the structure of a human being that consists of trillions of different types of cells that all work together for the maintenance of the entire organism. The cells perform basic, yet different functions that is essential for their own survival (1). These functions include the following: obtaining nutrients and oxygen from the environment surrounding the cell, providing energy to the cells by performing chemical reactions that use oxygen and nutrients, and waste removal of by-products produced during these chemical reactions to name a few (1). The processes that the body use to regulate its internal environment, is referred to as homeostasis (2). Homeostasis refers to the ability of an organism to maintain the internal environment (stability, equilibrium or balance) of the body, and is essential for the survival of each cell. Maintaining a stable internal environment requires constant adjustments as conditions changes both internally and externally (3). In other words, homeostasis defines a systems ability to uphold a constant internal environment in response to environmental changes (4). Examples of homeostasis include the balance between acidity and alkalinity, regulation of body temperature, and regulation of the glucose concentrations (5). The adjusting of physiological systems within a cell is called homeostatic regulation, also known as feedback regulation (6). The steps involved in this mechanism is: a) the sensor, which receives the information that something in the environment has changed, b) the integrating center, which receives and processes the information from the sensor, and c) the effector, which responds to the commands of the integrating center by either opposing or enhancing the stimulus (6). All of the body systems (such as the circulatory system, nervous system, and endocrine system) work together contributing to the homeostasis of the entire organism. Any disruption within one of the systems generally has consequences for the other body systems (1). The body system that is relevant for the rest of this master thesis is *the nervous system*.

### 1.1 The Nervous System

The nervous system, serves as the primary control center of the body working below the level of consciousness. For example, the hypothalamus of the brain is where the body's "thermostat/regulator" is found (1). The hypothalamus also stimulates the pituitary gland to

release various hormones that control metabolism and development of the body. The sympathetic and parasympathetic divisions of the nervous system alternatively stimulate or inhibit various bodily responses (such as heart rate, breathing rate, etc.) to help maintain proper levels (1). It also regulates various systems such as respiratory (controls pace and depth of breathing), cardiovascular system (controls heart rate and blood pressure), endocrine organs (causes secretion of ADH and oxytocin), the digestive system (regulates the digestive tract movement and secretion), and the urinary system (it helps adjust renal blood pressure and also controls voiding the bladder) (7).

The nervous system is comprised of two major parts, or subdivisions, the central nervous system (CNS) and the peripheral nervous system (PNS). The CNS includes the brain and spinal cord. The brain is the body's "control center". The CNS has various centers located within it that carry out the sensory, motor and integration of data. These centers can be subdivided to lower centers (including the spinal cord and brain stem) and higher centers communicating with the brain via effectors (7). The PNS is a vast network of spinal and cranial nerves that are linked to the brain and the spinal cord. It contains sensory receptors which help in processing changes in the internal and external environment. This information is sent to the CNS via afferent sensory nerves. The PNS is then subdivided into the autonomic nervous system and the somatic nervous system. The autonomic system has involuntary control of internal organs, blood vessels, smooth and cardiac muscles (1). The somatic system has voluntary control of skin, bones, joints, and skeletal muscle. The two systems function together, by way of nerves from the PNS entering and becoming part of the CNS, and vice versa (1).

The nervous system has three main functions, sensory input, integration of data and motor output. Sensory input is when the body gathers information or data, by way of neurons, glia and synapses. The nervous system is composed of excitable nerve cells and synapses connecting the cells to one another, to centers throughout the body or to other neurons (1). These neurons operate on excitation or inhibition and although nerve cells can vary in size and location their communication with one another determines their function (7). These nerves conduct impulses from sensory receptors to the brain and spinal cord. The data is then processed by way of integration of data, which occurs only in the brain. After the brain has processed the information, impulses are then conducted from the brain and spinal cord to muscles and glands, which is called motor output. Glia cells are found within tissues and are not excitable but help with myelination, ionic regulation and extracellular fluid. However,

recent research has shown that glial cells, which are about 10 times more numerous than nerve cells, also have certain chemical signaling functions, but lack the ability to generate nerve impulses (7).

The nerve outlets are of two kinds: dendrites and axons. With these, the nervous system is established as a very intricate network of interconnected cells. The dendrites are mainly the receiving apparatus for incoming signals from other nerve cells, while the axons and their branches are responsible for transmitting the signal to the next cell in the network. The nerve cells themselves thus become important nodes for processing and further distribution of the signals (1). An important signaling mechanism in this context is the nerve impulse. It has important functional consequences for the signal transmission in the nervous system: The signals can be disseminated quickly in cases where this is important (1). More numerous and slower conductive thin axons enable signal transmission of less urgent information across many channels simultaneously. Thereby, more information can be disseminated at the expense of slower transmission. The nerve impulses are short-lived so that new signals can be sent at short intervals. Thus, frequency coding (frequency of signal in a particular fiber) becomes an important factor in the dissemination of the information (1).

## **1.2 Synaptic transmission**

The axons most often divide into many branches. Each branch ends up in small buds (terminals, boutons) that are in intimate contact with other target cells, usually with their dendritic runners. Such specialized contact areas are called synapses, and their task is to mediate the signal transmission between nerve cells (1). There are two types of synapses that are recognized: the chemical synapse, and the electrical (8). The mode of neurotransmission is different between the two types of synapses. The electrical synapses, have the pre and postsynaptic membranes at a close proximity to each other and they are physically connected by channel proteins forming gap junctions (8). Whereas the chemical synapses transfer the information from one cell to an adjacent cell via the release of specific substances, called neurotransmitters (8). When a nerve impulse reaches the terminal, the neurotransmitter in the narrow gap is released at the contact site. It thereby allows to bind to specific receptors in the surface membrane of the recipient cell (the postsynaptic cell). When the neurotransmitter binds to the receptors, ion channels are opened in the postsynaptic membrane. The ionic current across the membrane leads to a change in the membrane potential and the signal is transmitted to the postsynaptic cell. These synaptic processes proceed rapidly, and most often are accomplished in a fraction of a second (1).

In the CNS, there are two main types of synaptic effects; inactivating (via the main neurotransmitter Gamma-aminobutyric acid (GABA)) and activating (via the main neurotransmitter glutamate) (1). Glutamate helps with the activation of the postsynaptic cells, by binding to the target receptor, which subsequently leads to an inwards depolarizing  $\text{Na}^+$  current in the postsynaptic cell. If the effect is sufficiently strong, it will trigger an impulse in the receiving cell – which is called an excitatory synaptic effect (9). On the other hand, the binding of GABA to the post-synaptic receptor ( $\text{GABA}_A$ -receptor) leads to an increase in the membrane potential (hyperpolarization) by having an influx of  $\text{Cl}^-$  occur (1).

### **1.3 Cell surface receptors**

The cell-surface membrane-bound receptors are mainly divided into two major groups: the ionotropic receptors and the G-protein-coupled receptors (10). The ionotropic receptors are relatively large, multi-subunit complex typically composed of four or five individual subunits that combine to form an ion channel through the membrane (11). The ionotropic receptors exist in a closed state in the absence of ligand/neurotransmitter, and does not allow the influx of ions. The binding of a neurotransmitters induces a rapid conformational change in the receptors, opening the channel permitting ions to flow down the electrochemical gradients (11). The changes in membrane current, as a result of ligand/transmitter binding to the receptors, are generally measured on a millisecond timescale (11). The ionotropic receptors include the AMPA and NMDA (N-methyl-D-aspartate), which are ionotropic glutamate receptors, and the  $\text{GABA}_A$ -receptor (12).

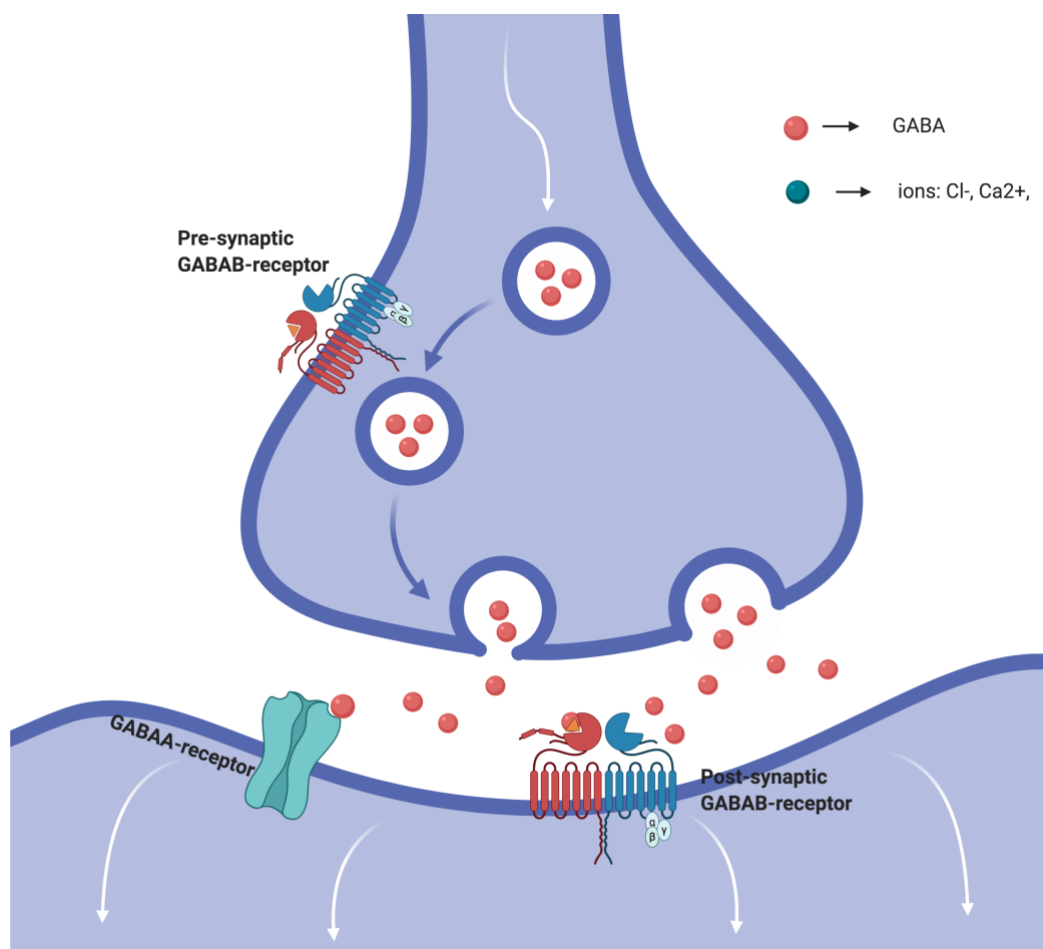


*Figure 1 A simplistic schematic presentation of the synaptic cleft and the pre and post synaptic GABAB receptors synapses. Model adapted from (13)*

#### **1.4 G-protein coupled receptors**

The G protein-coupled receptors (GPCRs) superfamily comprises the largest and most diverse group of membrane receptors in eukaryotes (14). This superfamily includes the muscarinic acetylcholine receptors, adrenergic receptors and opioid receptors. The GPCRs are targeted by some of the most commonly used drugs. Studies have shown that approximately 30% of all drugs binds to these receptors and therefore an increased understanding of these receptors has greatly affected modern medicine (15)

These GPCRs are embedded in the cell membrane and are responsible for transducing signals from extracellular stimuli to intracellular responses through multiple downstream effectors, such as the G-proteins and beta-arrestins (16). The GPCRs are different from the ionotropic receptors, both structurally and functionally. Where the ionotropic receptors have their channel

portion linked with the ligand binding site, this is not the case for the GPCR (17). The GPCRs give their effects via intracellular proteins, and affect the channels indirectly through the downstream effectors. The number of steps required for the GPCRs to produce a response, is the reason for why the activation takes a longer time compared to the ionotropic receptors (17).

GPCRs are also distinguished by their unique structure consisting of an extracellular N-terminus where the ligand binding site is found, the heptahelical transmembrane domain (7TM), and the intracellular C-terminus (18). The exact percentage of GPCRs that the human genomes codes for is not fully known, but a study (19) estimates that approximately 4% of the human genome codes for GPCRs giving us more than 800 subtypes (20).

### **1.1.1 Activation of the GPCR**

Activation of these receptors is controlled by the binding of extracellular signal in the form of e.g. drugs or endogenous ligands (21). Receptor activation then induces a cascade of reactions, including conformational change, which in turn will activate the G-proteins (22). The G-proteins (guanine nucleotide-binding proteins) are a group of proteins that acts as “molecular switches” inside cells, and activates a cascade of further signaling events that finally results in a change in cell function (23). These proteins are heterotrimeric, consisting of three subunits: alpha, beta and gamma. Both the alpha and gamma subunits have covalently attached lipid tails that help anchor the G-protein in the plasma membrane (23,24). In the absence of extracellular stimuli, the alpha subunit is attached to GDP and the G-protein is inactive. Whereas an active conformation of the receptor induces a change in the alpha subunit causing the exchange between the GDP and GTP (25). The alpha subunit attached to GTP will then dissociate from the activated beta-gamma complex, and these two separate complexes will go on to do their jobs respectively (25).

The activated alpha-subunit goes on to regulate to a membrane bound enzyme that catalyzes a reaction that produces “second messengers” that act like an amplifier of the first signal sent by the ligand (26). The second messengers are in many cases produced by the activation of protein kinases, that phosphorylate target proteins and alter their activity carrying out the biological response of the cell, to the ligand (21,26). The alpha subunit has a GTPase activity and as such, cleaves GTP to GDP which in turn triggers the deactivation of the G-protein and the reassembly of the subunits (23).

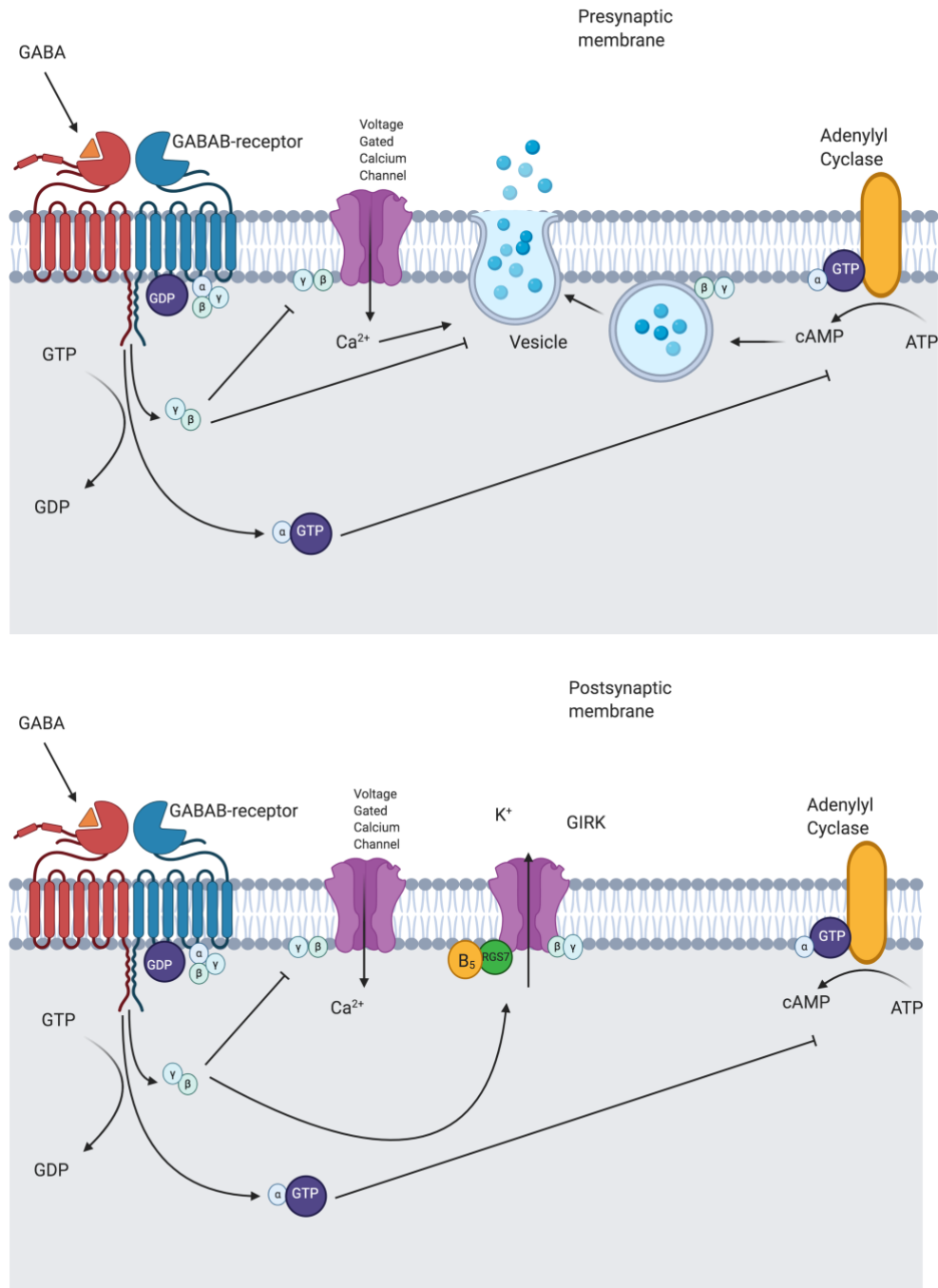


Figure 2 These figures shows the regulation of neuronal GABA<sub>B</sub> receptor functions by subunit composition in a) the presynaptic membrane and b) post synaptic membrane. Figure adapted from (27)

### 1.1.2 Beta-arrestin signaling pathway

The arrestins are multifunctional adaptor proteins that associate with various cell surface receptors and regulate transmembrane signal transduction (28). The arrestin family consists of four members: a) arrestin 1, b)  $\beta$ -arrestin1, c)  $\beta$ -arrestin2, and c) arrestin 4 (28). The  $\beta$ -arrestins

( $\beta$ -arrestin1 and  $\beta$ -arrestin2) were previously thought to only inhibit the signal transduction because they competed with and blocked the binding of the G-proteins to the 7TMs (28,29). But as for now, the  $\beta$ -arrestins are appreciated as multifunctional adaptors that mediate trafficking and signal transduction of the 7TMs and other receptors, in addition to their role as desensitizers (29). They desensitize the second messenger signaling through distinct protein-protein interactions; by scaffolding phosphodiesterases and diacylglycerol kinases,  $\beta$ -arrestins promote the degradation of cAMP and diacylglycerol (29).

The binding of  $\beta$ -arrestins requires a specific phosphorylation signature on the receptor's intracellular domains, which is created by specialized serine-threonine kinases called G-protein coupled receptor kinases – GRK for short (28). The phosphorylation of activated GPCRs, is known to be a critical regulatory mechanism, which initiates a variety of downstream effects by engaging different conformations of  $\beta$ -arrestins and promoting their various functions (29).

### **1.5 Classification of the GPCR**

Various classification systems have been used to organize the receptors. Currently, the A-F system is widely used and is mainly based on their amino acid sequences and functional similarities (30). This system is designed to include all the known GPCRs from both vertebrates and invertebrates, which means that some of these groups are not found in mammals. This led to the proposed creation of the GRAFS classification system, which divides vertebrate GPCRs into five families/classes and named after the family names: Glutamate (family C), Rhodopsin (family A), Adhesion, Frizzled/Taste2 (family F), and Secretin (family B) (31).

The class A (rhodopsin-like receptors) is the largest group of GPCRs, which includes the light receptors, chemokine receptors, 5-hydroxytryptamine (5-HT, aka serotonin) receptors, and accounts for around 80% of the GPCRs (32). The first high-resolution X-ray structure of a GPCR, that of Rhodopsin, was obtained in 2000 (33). Most of the experimentally solved structures of GPCR are of the class A family and this sparked an interest to determine the 3D structures within the class C family.



## 1.6 Class C GPCR

This class of GPCRs from humans is constituted by eight metabotropic glutamate receptors,  $\gamma$ -aminobutyric acid-b receptors (GABA<sub>b</sub>), and Ca<sup>2+</sup>-sensing receptors (CaS receptors) to name a few. These receptors represents an important new class of therapeutic drug targets that are fundamental to disorders that affect the CNS (34). As mentioned earlier, GPCRs are well recognized for their conserved heptahelical transmembrane domain, and among these families, the class C GPCR is characterized by their large extracellular domain and contains the orthosteric site namely the Venus flytrap (VFT) and the cysteine rich domain (CRD) - although the CRD is not present in the GABA<sub>b</sub> receptor (34).

The orthosteric binding site for class C GPCR is located in the VFT, whereas the binding site for class A GPCR is located within the 7TM. Class C GPCR exhibits unique features/characteristics including an allosteric binding site and the mandatory dimerization. So far, there are only two therapeutic drugs that target class C GPCRs: the GABA<sub>b</sub> orthostatic ligand Baclofen, and a CaS receptor positive allosteric modulator Cinacalcet (34).

## 1.7 Allosteric modulation

Allosteric modulators of GPCRs bind to sites that are often less conserved than orthosteric sites, and this has allowed for the optimization of highly selective allosteric modulators of some GPCR subtypes (35). The allosteric modulators can be categorized into three subgroups based on their activity. **Positive allosteric modulators** (PAMs) bind to the allosteric binding site, and increase the response of the orthosteric ligand (for example Cinacalcet) (35). Some of the PAMs have been shown to induce an effect on the receptor without the presence of an orthosteric ligand, and these modulators are referred to as agonist-PAMs (agoPAM) (36). **Negative allosteric modulators** (NAMs) have a direct opposite effect of the PAMs, where they reduce the response of an orthosteric ligand (35). The drug Maraviroc is a NAM that works on the class A receptor CCR5 (37). **Neutral/silent allosteric ligands/modulators** (NALs/SAMs) bind to the allosteric site but does not alter the ligands activity. The SAMs may prevent other modulators to bind to the same place, depending on where they bind, thus inhibiting their modulation (38).

The search for new allosteric modulators has been intensified, due to the difficulties in designing orthosteric drugs that are safe and effective in drug therapeutics (39). Allosteric

modulation has been adopted as an innovative tool that can provide precision targeting of GPCRs and increasingly utilized throughout the past decade (39).

### 1.8 Metabotropic glutamate receptors (mGluRs):

Metabotropic glutamate receptors (mGluRs) belong to the Class C G-protein-coupled receptor and are activated by the main excitatory neurotransmitter glutamate. The widespread expression of mGluR, in particular, mGluR1 and mGluR5 subtypes, throughout the central nervous system has made those two receptors attractive therapeutic targets for the treatment of severe neurological disorders, such as schizophrenia, anxiety, Parkinson's disease and major depressive disorders (40). The mGlu receptors exist as either homo or heterodimers.

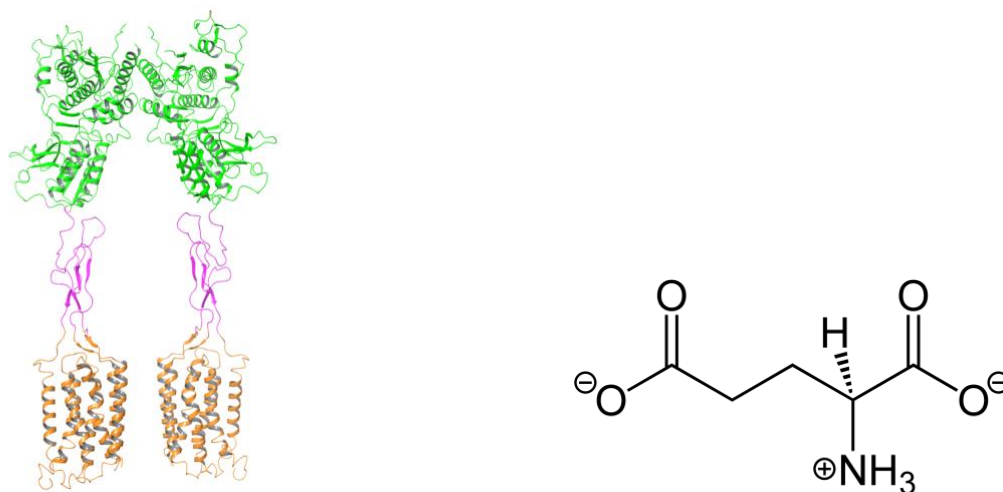


*Figure 3 a) CryoEM structure of the mGlu5 receptor (PDB:6N52). The parts coloured in green represents the extracellular VFT domain, the parts in pink represents the CRD and lastly the structures in orange represents the 7TM domain b) the chemical structure of glutamate.*

There are eight different types of mGluRs (mGlu1-8), divided into three groups based on the overall structure and physiological activity: Group 1 (mGlu1 & mGlu5), Group 2 (mGlu2 & mGlu3) and Group 3 (mGlu4, mGlu6, mGlu7 & mGlu8).

The mGlu1 and mGlu5 receptors, are the only experimentally determined structures we have of the class C GPCRs, but there's been an increased effort in solving the three-dimensional structure of GABA<sub>B</sub> with cryoEM (41). Structural insight of these receptors shows that the activation of these receptors are more complicated than for the class A GPCRs. They form obligate dimers and possess the extracellular Venus flytrap domain, which are linked to the

CRD – which works as a linker between the 7TMs and the VFT (42). The oligomerization of the GPCRs have been of interest for a long time, but the complexes have been difficult to observe and analyze both structurally and biophysically within the class A and B GPCRs (43).

The binding of an orthosteric agonist leads to two major structural changes in the conformation of the dimer (44). The first change is a closure of the two VFTs, where a signaling study (45) in live cells have suggested that the VFT closure is important for the activation (44). It is also suggested that closure of one lobe is sufficient for signaling, whereas closure of both lobes is necessary for full efficacy (46). The second major change involves a reorientation of the intersubunits, that brings the CRDs of the adjacent VFTs into near proximity to each other (44). This dimerization process is required for the G protein activation.

### 1.9 GABAergic system

GABA is the main inhibitory amino acid neurotransmitter of the mammalian central nervous system, and is synthesized from glutamate by glutamate decarboxylase (GAD) in the presynaptic neuron (47). GABA is released from the synaptic vesicles into the synaptic cleft, where it binds to its postsynaptic receptors. This binding induces a response, which results in the neuron being hyperpolarized (48). The leftover GABA in the synaptic cleft are transported back to the presynaptic neuron and glia cells, by the GABA transporters – also known as GAT (49).

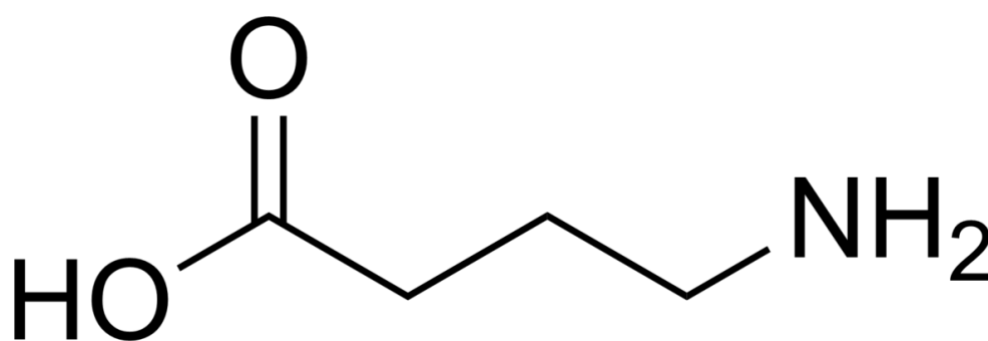


*Figure 4 The chemical 2D structure of GABA.*

Due to GABA modulating the majority of inhibition that is ongoing in the brain, the disruption in the GABAergic inhibition have the potential to result in seizures (48). Other

disorders such as psychiatric disease, spasticity, and stiff-person syndrome have all been related to the disorders of GABAergic function in the brain (48)

The GABA-receptors can be divided into two classes; ionotropic receptors (GABA<sub>A</sub> and GABA<sub>C</sub>) and the metabotropic receptor GABA<sub>B</sub>. The GABA<sub>A</sub> is an ionotropic receptor. These receptors consists of five subunits arranged around in a circle to form a pore/channel that remains closed until GABA binds to the active site (48). The subunits are called  $\alpha 1$ ,  $\beta 2$ , and  $\gamma 2$ , where the GABA binding sites are found between the  $\alpha 1$ - $\beta 2$  subunits and the benzodiazepine binding site is found between the  $\alpha 1$ - $\gamma 2$  subunits. The binding of GABA, causes the pores to open up and allows the Cl<sup>-</sup> ions into the nerve cells. Influx of Cl<sup>-</sup> ions will then hyperpolarize the nerve cells, causing it to stop firing signals (49).



*Figure 5 a) the membrane view of the GABA<sub>A</sub> receptor (PDB: 6D6T) and b) the top view of GABA<sub>A</sub> receptor, where all the subunits are represented in different colors. Models made in Maestro*

The GABA<sub>B</sub> receptor was discovered in 1979, by the late Dr. Noman Bowery (50). While the ionotropic GABA-receptors are ligand-gated ion channel that mediates large and quick neuronal inhibition, GABA<sub>B</sub> acts slowly and has a delayed action. The reason being from it relying on the G-protein to mediate its response. The GABA<sub>B</sub> – receptor signaling involve one of three effector proteins: voltage-gated Ca<sub>2+</sub> channels, G-protein-activated inwardly-rectifying K<sup>+</sup> channels (GIRK) and adenylyl cyclase (51). The GABA<sub>B</sub> receptors have different functions depending on where they are located. Located on the presynaptic neuron, the GABA<sub>B</sub> receptor can influence the release of neurotransmitters, by decreasing the Ca<sub>2+</sub> influx through the voltage-gated Ca<sub>2+</sub> channels. This leads to a reduction of neurotransmitter release at both excitatory and inhibitory synapses (52). Additional mechanisms may include

the opening/activation of  $K^+$  channels which in turn prohibits the influx of  $Ca^{2+}$  and/or by decreasing the cAMP concentrations which is important for the vesicle priming (51,52). The postsynaptic effects are exhibited when the receptors activate the G-proteins, which in turn reduces the activity of adenylyl cyclase. This causes a decrease in  $Ca^{2+}$  conductance, and an increase in  $K^+$  inductance (51,52).

GABA<sub>B</sub> is an obligatory heterodimer, with two subunits (GABA<sub>B1</sub> and GABA<sub>B2</sub>) specialized for different functions. Each subunit consists of three domains: an N-terminal extracellular domain, 7TM domain and a cytoplasmic tail (53). The ectodomain structure has also been determined in multiple conformations, allowing us to describe the heterodimer interfaces, receptor-ligand interactions, and conformational changes associated with receptor activation (54). GABA<sub>B1</sub> is needed for the activation by an external agonist, while the GABA<sub>B2</sub> subunit is responsible for both signaling and membrane targeting (52). The allosteric binding site of the allosteric modulators seems to be in the GABA<sub>B2</sub> subunit (55). GABA<sub>B</sub>, like other class C GPCRs, can be regulated by allosteric modulators. The first PAM of the GABA<sub>B</sub> receptor, CGP7930 was discovered through drug screening, and since then search for new allosteric modulators has intensified (56).

Currently, baclofen is the only marketed drug that targets the GABA<sub>B</sub> receptor, and is used to treat spasticity. The drug which is given orally, does not penetrate the blood brain barrier easily and thus binds to other receptors in the body, causing a lot of adverse effects (57). It has therefore been a goal for the pharmaceutical industry to either develop more potent drugs that may cross the blood brain barrier easier, and because of this only small dosage of the drug will be needed.

### **1.10 Allosteric modulation of the GABA<sub>B</sub> receptor**

The GABA<sub>B</sub> have been used as a target in high throughput screening strategies where the end goal is to identify new allosteric modulators acting at these receptors (56). A previous study following the molecular characterization of the GABA<sub>B</sub> receptor heterodimer indicated that  $Ca^{2+}$  ions act as enhancers of this receptor (58). Another study observed that a few hundred micromolar of  $Ca^{2+}$  increased the potency of GABA in stimulating GTP $\gamma$  S binding or G-protein activation measured in second messenger assays (59).

A few years before this observation, a number of allosteric modulators of the other class C GPCRs, especially mGlu receptors, were identified, including both negative and positive

allosteric modulators (56). What they discovered was that both the PAM and NAM were found to bind in a cavity within the transmembrane domain, contacting the residues of TM3, TM5, TM6 and TM7, a site that is clearly distinct from the orthosteric binding site (60,61).

These observations sparked an interest for the pharmaceutical companies to search for new GABA<sub>B</sub> modulators, using high throughput functional assays (56). As for now, only two PAMs have been reported in the literature: CGP7930 (2,6-Di-tert.-butyl-4-(3-hydroxy-2,2-dimethyl-propyl)-phenol) and GS39783 (N,N'-Dicyclopentyl-2-methylsulfanyl-5-nitro-pyrimidine-4,6-diamine) (56).

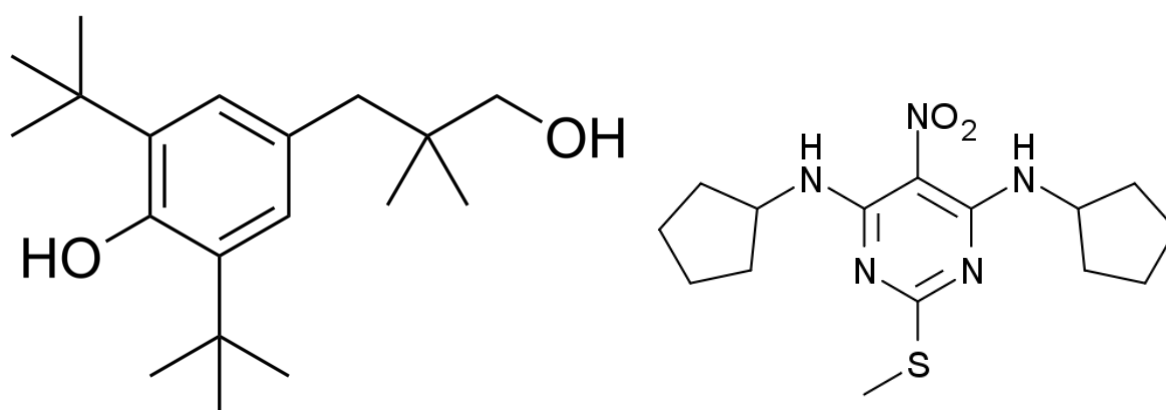


Figure 6 The 2D chemical structure of the PAMs a) CGP-7930 and b) GS39783

These two PAMs were found to enhance agonist potency as well efficacy on recombinant GABA<sub>B</sub> receptors in various assays (56). A previous study (62) identified the mode of action for CGP7930, on various combinations of wild-type and chimeric GABA<sub>B</sub> subunits, and took the advantage of the agonist activity of the PAM in their assay (56). This study revealed that the PAM was found to activate GABA<sub>B2</sub> subunit expressed alone, as well as a shortened version of this subunit corresponding to the transmembrane domain only (56,62). Another study (63) tried to identify the mechanism of action using chimeric drosophila/rat subunits (63). They managed to bring further evidence for GS39783 acting in the transmembrane domain of the GABA<sub>B2</sub> subunit, but they weren't successful in identifying the residues in the 7TM that were important for the interaction (62). Although they weren't able to find any

important residues, mutations in the TM6 were found to convert the modulator into an agonist, suggesting that the mutated residues are involved in stabilizing the GABA<sub>B</sub> 7TM into its inactive conformation (56,63).

In summary, the findings on the GABA<sub>B</sub> receptor illustrate the power of allosteric modulators, and how they are excellent alternatives to Baclofen for a number of therapeutic applications (56)

### **1.11 Molecular modelling**

The emergence of computational based methods has helped tremendously in the discovery and development of new drugs. Rapid advances in computer hardware and software have meant that many of the operations that once were exclusive province of the experts, can now be done by ordinary laboratory computers (64). Molecular modelling is a collection of computer based techniques for deriving, representing and manipulating the structures and reactions of molecules and those properties that are dependent on these three-dimensional structures (3D) (65).

### **1.1.3 Molecular and quantum mechanics.**

The computational methods that are used to calculate structure and property data, can be split into two categories: quantum and molecular mechanics (64). As the name implies, **quantum mechanics** (QM) uses quantum physics to calculate the properties of a molecule by utilizing the Schrodinger's equations to calculate the energy. The movements of the electrons of an atom relative to the nucleus is taken into account, and its therefore possible to derive properties that depend upon the electronic distribution. This gives a more precise description of the electronic structure of the molecule than the molecular mechanical approach and will normally give a more accurate prediction of the geometry and energy. However, QM calculations are very time-consuming, and therefore limited to small systems (i.e. a few hundred atoms) (66). For that reason, molecular mechanics is preferred.

**Molecular mechanics** (MM) utilizes equations that follows the laws of classical physics and apply them to the nuclei and ignores the electronic motions, known as the Born-Oppenheimer approximation (67). The rotational and vibrational movements of the entire molecule are mainly dependent on the movements of the atomic nuclei, and each atom can be treated as series of spheres/particles. Molecular mechanics is fast and less intensive on computer time than QM. However, it cannot calculate electronic properties because electrons are not included in the calculations. Therefore, a combination of MM and QM model description can

be used. A description of the active site regions of the protein can be done by using a quantum mechanical model description, whereas the remaining regions of the protein can be described by using molecular mechanics (66).

#### **1.1.4 Force fields**

In molecular mechanics, the force field consist of mathematical formulas that describe the interactions between particles. The total energy ( $E_{\text{tot}}$ ) of a system is calculated by summing the different forces involved in the covalent and non-covalent interactions of the system ( $E_{\text{Bonded}}$ ) and ( $E_{\text{Nonbonded}}$ ) (68). The force field can therefore be written as:

$$E_{\text{tot}} = E_{\text{Bonded}} + E_{\text{Nonbonded}}$$

where

$$E_{\text{Bonded}} = E_{\text{Bond}} + E_{\text{Angle}} + E_{\text{Dihedral}} \text{ and } E_{\text{Nonbonded}} = E_{\text{Electrostatic}} + E_{\text{VanderWaals}} \text{ (68)}.$$

#### **1.1.5 Energy minimization**

The goal of all molecules is to find the right conformation, with the lowest energy (minimal energy strain), as they are the most stable in this form (64). Whenever a 3D structure is created, with the help of computational methods, the next rational step would be the energy minimization. This process is necessary, because the construction process may have resulted in unfavorable bond lengths, or bond/torsional angles and these changes will have a huge effect on the overall energy of the entire molecule (64). The output of this calculation, is a new structure where the bond lengths, bond/torsional angles are recalculated to make it more energetically more stable.

#### **1.1.6 Homology modelling**

Having the amino acid sequence of a protein is not the same as knowing the overall fold of the protein or knowing the function of the protein. To understand the functional mechanisms of a protein, having the 3D structure is important. The 3D structure of a protein can be experimentally determined by using X-ray crystallography, NMR-spectroscopy or cryogenic electron microscopy (cryoEM) (69).

In cases where the 3D structure of a protein is not known, mainly due to the difficulties of determining the overall structure of the membrane proteins, a prediction method can be useful (70). Homology modelling is a prediction technique used to construct 3D structures of an



unknown macromolecule from a homologous macromolecule (macromolecules that share the same ancestor) with known 3D structure, due to the difficulties to determine the real 3D structure (70). This approach takes advantage of the fact that the hydrophobic core of membrane proteins is preserved since only small changes in amino acid sequence is tolerated in order to maintain the overall fold. The core is mostly made up by secondary structure elements, that are necessary for building the scaffold. The steps in homology modelling are: Step 1) template search, step 2) template and target alignment, step 3) model construction and step 4) model evaluation (71).

The template search is the initial step in which a program/server compare the sequence of an unknown structure with a sequence with known structured stored in PDB (70). The most popular server is BLAST (Basic Local Alignment Search Tool), and a search with this server against the database for optimal local alignments with the query, gives a list of known protein structures that matches the sequence. This method only works when the sequence identity is above 30%, as the homology hits become more unreliable when the sequence identity is below this percentage (70). In the case of low sequence identity, choosing multiple templates can improve the quality of the model when compared to using only a single template (72).

Once the template is selected, a target-template alignment is performed by using unique pairwise or multiple sequence alignment tools (72). This step is very delicate as mistakes during this step may cause the generation of an incorrect homology model. The model building step consists of the backbone generation, loop modelling and side chain modeling. The program ICM, uses an automated method that inherits the backbone from the aligned (not necessarily identical) parts of the template and adds the extracted side chain conformations for residues identical to the template (73). The non-conserved loops are inserted based on conformational database searches with matching loop ends, and upon insertion into the model non-identical side chains are assigned the most likely rotamer and optimized by torsional scan and minimization (73). Model evaluation can be done using the Structural analysis and verification server (SAVES), which is used for stereochemical evaluation. The Ramachandran plot is one of the tools found on the server, that can help with the validation of the constructed models.

The Ramachandran plot, also referred to as the Ramachandran diagram, is a 2D-plot of the phi ( $\phi$ ) and psi ( $\psi$ ) torsion angles of the protein backbone, and it basically provides a simple view of the conformation of the specific protein, identifying if it has too many outlying

residues (74). The phi and psi angles cluster into defined regions in the plot where each region corresponds to a particular secondary structure (74). The main use of this plot is to visualize the energetically allowed and forbidden regions. For many poor quality homology models, many dihedral angles are found in the forbidden regions of the plot – and such deviations usually indicates problems with the structure (75).

In addition to that, the binding of decoys (non-binders) may also prove useful in the assessment of model quality.

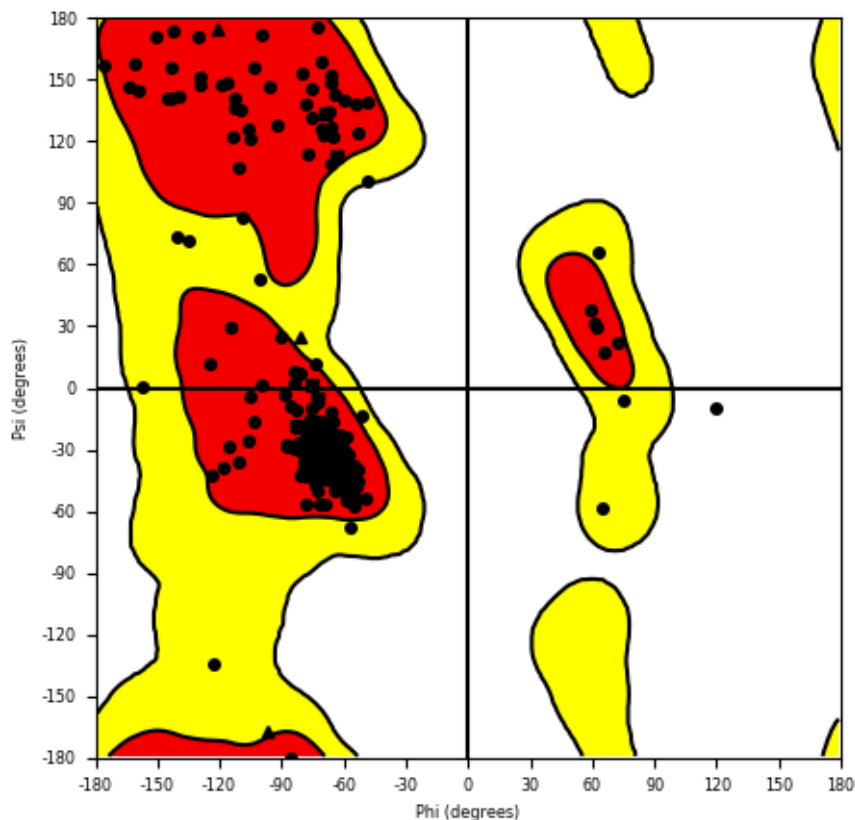


Figure 7 Ramachandran plot for a constructed homology model. The plot shows the placement for each of the residues in the protein backbone. The red regions represent the allowed region, where there are no steric clashes. The yellow regions represents the additional allowed regions if slightly shorter van der Waals radii are used in the calculations, and the white regions are the so called disallowed regions, which generally involve steric hindrance between the side chain C-beta methylene group and main chain atoms (76). This plot was made using Schrödinger's Maestro

Lately, there have been a growing trend with solving the 3D structure of membrane proteins using cryoEM method. This method brings a number of desirable features to structural biology that weren't available before (77). The technique allows macromolecules to be studied in "native" conditions (i.e. biochemically functional buffer conditions), as opposed to the classical X-ray crystallography method (77). It also provides the opportunity to determine structures for macromolecules in many functional states that are in equilibrium with one another (77).

### 1.12 Drug design

The development of new drugs is a long and costly process, where the overall goal is to discover high potency and high affinity molecules. In the earlier years, the early stage of drug discovery involved testing compound with the emphasis on identifying biological activity. This approach has in many recent drug discovery campaigns, been neglected as lead compounds are now designed with increased emphasis on information obtained from 3D structures of a biological target/ligands (78). Using such 3D-structural guided drug design is often referred to as rational drug design (78). Rational drug design can be divided into two approaches: structure-based drug design (SBDD) and ligand-based drug design (LBDD).

**Ligand-based drug design** is the approach used to design drugs based on the ligands physiochemical properties, when the 3D-structure of the target is unknown. LBDD utilizes certain parameters to identify the structure-activity relationship (SAR). The most looked at parameters includes: pharmacophores, fingerprinting and Q-SAR.

A pharmacophore is defined as "the ensemble of steric and electronic features that is necessary to ensure the optimal supramolecular interactions with a specific biological target structure and to trigger (or to block) its biological response" (79). However, it does not represent a real molecule or a real association of functional groups, but is purely an abstract concept that accounts for the common molecular interaction capacities of a group of compounds towards their target structure (80). Typical pharmacophoric features/sites includes: hydrogen binding acceptor/donor (HBA/HBD), a negatively charged group (anions), a positively charged group (cations), an aromatic ring and hydrophobic groups (27). The pharmacophore model highlights the functional groups involved in the interaction with the

target, the nature of the non-covalent bonding and the different interchange distances. It should also show predictive power and lead to the design of new, more potent compounds or, even better, of totally novel chemical structures (28).

On the other hand, QSAR (quantitative structure-activity relationship) is defined as "mathematical relationship linking chemical structure and pharmacological activity in a quantitative manner for a series of compounds" (83). A QSAR has the form of a mathematical model: Biological activity = f(physicochemical properties + structural properties), and the properties used in the calculations are properties that are easy to quantify: hydrophobicity, electronic descriptors and steric descriptors (84)

The 2D fingerprints are widely used in drug discovery and have been shown to be more successful in obtaining active compounds than 3D shape or docking methods (85). The reason for that is because it's based on the similarity property principle, which states that molecules with similar structure and properties, are most likely to exhibit similar activity (86). They encode the presence of 2D substructural fragments in a molecule, such as atom and bond types (86). In 2D fingerprint-based screening, the fingerprints are constructed based on the reference ligand(s) and the ligands from a library, and a similarity metric method is used to calculate the degree of resemblance/similarity between the fingerprints (86). The Tanimoto coefficient/index (Tc) is the most used similarity metric in the literature (85). The Tanimoto index is defined as:

$$c/(a+b-c)$$

where  $a$  is the number of fragments in compound A,  $b$  is the number of fragments in compound B, and  $c$  is the number of fragments in both compounds (85).

**Structure-based drug design** is a strategy used to design drugs based on the knowledge of the known 3D-structure of the target. In other words, SBDD takes advantage of the properties of the target to identify/create a complementary drug.

Docking is referred to as the process where a program place the atoms or fragments/ligands into the target, while scoring is the calculations of the binding affinity of a docked

conformation (78). The goal of docking is to produce a protein-ligand complex, which resembles a "native" complex in the biological system and the goal of scoring is to calculate the binding energy or affinity between a target and ligand in a native complex (78). It is important to note that the docking procedure will just produce the theoretical" best" ligand-target complex; which means that this approach does not necessarily represent the true binding mode. The binding energy ( $\Delta G$ ) is the sum of both enthalpic and entropic contributions and is written as:

$$\Delta G = \Delta H - T\Delta S \text{ (Gibbs free energy)}$$

The early docking programs considered both the target and the ligand as rigid entities, but has now been replaced by the flexible ligand and rigid receptor induced fit protocol which assumes that the original structure of a target may not fit a ligand exactly, but rather that the ligand induces a conformational change in the target upon binding (78).

### 1.1.7 Virtual Screening (VS):

The increased economic pressure on the pharmaceutical industry to develop new drugs in a faster and more efficient way, has led to the development of a large number of new methods aimed at a more efficient and rapid lead structure discovery process. Recent advances in combinatorial chemistry have made it possible for chemists to synthesize large libraries of compounds, and today high-throughput screening (HTS) allows considerable reduction of the time amount needed for the discovery of new molecules possessing biological activity for a certain target. However, the number of compounds that can be synthesized is still a small percentage of the total number of compounds that are possible in principle (87). Lack of lead-compounds calls for identification of new ligands using experimental or **computer-based methods**. **Computer-based methods** include *virtual screening* and de novo design. The compounds obtained from the virtual library, may have different sources. The compounds in this virtual library represents real compounds, with one example being the Drugbank (88).

In recent years, the focus on drug repurposing has increased. Drug repurposing is an approach used to accelerate the drug discovery process through the identification of a new indication for an existing drug approved for a different indication (89). This method capitalizes on the fact that approved drugs and many abandoned compounds have already been through the clinical tests in animal and humans (90). Drug repurposing has many advantages, one being

that it can significantly reduce the cost and development time compared to the traditional de novo drug discovery approaches (90).

## **2 Aim**

The aim of this study was to primarily 1) find new allosteric modulators to the GABA<sub>B</sub> receptor, by learning how to use in silico methods like virtual screening. The databases used for this purpose were Molport and Drugbank. The Molport database was screened by using both the LBVS and SBVS approach based on a PAM found in an in-house study , while the DrugBank screening was performed as an attempt to find new indications for already established drugs.

2) to screen the compounds against the built homology models of the GABA<sub>B</sub> receptor to investigate possible interactions in the binding pocket and 3) to learn how to run experimentally functional in vitro assays to assess the effects the test compounds may have on the cAMP.

### **3 Methods**

#### Part I: In Silico

##### **3.1.1 Software packages**

###### **3.1.1.1 Molsoft Internal Coordinate Mechanics (ICM) Software (version 3.8-7c)**

ICM is a programming environment for various tasks in computational chemistry and computational structural biology. It was used to build multiple 3D models (homology models) of the target.

###### **3.1.1.2 Schrödinger Maestro (software package version 12.2.012, release 2019-3)**

Schrodinger Maestro is a graphical user interface (GUI).

###### **Schrödinger LigPrep (software package version 12.2.012, release 2019-3)**

Schrödinger Ligprep is an application in Maestro, used to generate 3D structures of ligands, from 2D structures. The LigPrep protocol produces low-energy 3D structures with the correct chirality for each input structure. It also has the ability to produce a number of structures from an input structure with various ionization states, tautomers, stereochemistry, and ring conformations (91). LigPrep was used to convert DrugBank, and Molport, to get a more accurate representation of the compounds, and enable it for use with other applications (such as Glide docking).

###### **Schrödinger Glide docking (software package version 12.2.012, release 2019-3)**

The Glide docking package was used to dock the selected databases, primarily using two different protocols. The SP (standard precision) docking protocol was used on all compounds (from all databases), as it was made to dock a large number of compounds with high speed and accuracy (92). This protocol is more “forgiving” compared to XP docking, as it is adept at identifying ligands with a reasonable inclination to bind, even if the Glide pose has imperfections (93). The XP (extra precision) docking protocol was only used for a few compounds of interest, as this protocol is recommended for a small amount of compounds (92). The XP docking protocol penalizes poses if they violate established physiochemical principles, such as when charged polar groups are exposed to solvents, and the main goal of this protocol is to rank a ligands ability to bind to a specific receptor conformation (92).



### **Schrödinger QikProp (software package version 12.2.012, release 2019-3)**

QikProp is a tool used to calculate/predict the ADME (absorption, distribution, metabolism, and excretion) properties of compounds. It is also a useful tool that plays a vital role during lead generation and lead optimization.

### **Schrödinger Canvas (software package version 4.2.012)**

Canvas is a tool used for cheminformatics with a range of applications including structural and data analysis. It utilizes cheminformatics techniques such as fingerprint-based similarity searching and substructure matching, that can screen a huge amount of compounds (from various databases); while the use of clustering and diversity selection can analyse and improve the content of real and virtual libraries.

## **3.1.2 Databases**

### **3.1.2.1 UniProtKB – The universal protein resource**

UniProt Knowledgebase is a freely accessible database of protein sequence and functional information. The primary protein sequence of GABA-B2 (Entry ID: O75899) was retrieved/obtained from UniProt/Swiss-Prot and manually adjusted to include only the 7TM domain of the receptor complex.

### **3.1.2.2 DrugBank**

DrugBank is a free database containing comprehensive information about drug and drug targets (88). The drugs are categorized based on their status (approved, nutraceutical, illicit, investigational, withdrawn and experimental) and market availability. The range and variety of drugs in this database make it not only a good source of virtual screening, but it also serves as an opportunity to discover new therapeutic indication for some drugs (repurposing). Since its release in 2006, DrugBank has extensively been used to facilitate in silico drug target discovery, drug design, docking, screening, drug interaction and general pharmaceutical education (88).

Four of the subsets from DrugBank (approved, illicit, metabolites and withdrawn), downloaded from the site on the 24<sup>th</sup> of October 2019, were used for the pursuance of new potential positive allosteric modulators (from already approved drugs) for the GABA<sub>B</sub> receptor. The total number of compounds was around eleven thousand.

### 3.1.2.3 Molport

The Molport database is a freely accessible and commercial chemical marketplace that lists millions of compounds from multiple vendors. Its practicality makes it a good source for virtual screening in search of new hit compounds. The subsets (which included approximately 7 million compounds) were downloaded from the Molport database on the 26<sup>th</sup> of November 2019. This database was used to screen for new analogues based on the reference PAM TI-400 (a potential PAM as a result from a previous in-house study)

### 3.1.3 Homology modelling

A homology modelling step was performed due to the lack of a solved three-dimensional structure of the GABA-B2 receptor, and it was done in a four-step process.

#### Step 1: Template selection

Four active-like conformations of the metabotropic glutamate receptor were selected as templates to construct the 7TM domain of the GABA-B2 subunit. The templates had been obtained by running a molecular dynamic (MD) simulation on the mGlu1 receptor including an agoPAM by Thibaud Freyd et.al (manuscript in preparation).

#### Step 2: Target-template sequence alignment

The sequence-based alignment step was performed in ICM by using aligning the amino acid sequence of the active-like mGlu1 and the manually adjusted GABA-B2 (UniProtID: O75899), to fit a published sequence alignment (42). The alignment can be found in Appendix.

### Step 3: Model building and refinement

Four models were generated based on the mGlu1-GABA-B2 sequence alignment and refined entering the commando “refineModel 5 yes” in the terminal. This commando enabled ICM to refine the models by globally optimizing the side-chain positions and annealing of the backbones (94). The commando includes three steps: 1) a Monte Carlo simulation of the side chains, 2) five steps of iterative annealing of the backbone structure, and 3) a second Monte Carlo simulation of the side chains (94).

### Step 4: Evaluation of the models

The last step of homology modelling was the evaluation phase. This phase was divided into two separate stages: a) Protein Preparation (Ramachandran plot) and b) docking of decoys and PAMS

The first step was to export the constructed homology models to Schrödinger Maestro, and perform a protein preparation, to make sure the generated models fit the force field created by the program. The defaults settings were used, and in this step: force field atom types and bond orders were assigned, missing atoms were added, protonation states were predicted, H-bond networks were optimized, water orientations were sampled, and the ionizable residues (Asparagine, Glutamine, and Histidine) had their flip state sampled to optimize the hydrogen bond network (95,96). The models were then energy minimized.

The models were then reviewed by analyzing the Ramachandran plot in, to see if some of the amino acids were placed outside of the energetically favorable region, as this could be used as an important factor in the assessment of the quality of the built homology models.

The second step involved the docking of decoys and GABAB receptor PAMs. This step was done to ensure that the built models bound a higher number of the PAMs (so-called known binders) and at the same time filter out the decoys (non-binders that are presumed inactive compounds). The docking protocol were done in three steps: 1) ligand preparation, 2) receptor setup, and 3) docking & scoring.

### 3.1.4 Ligand preparation

72 unique PAMs were obtained from the literature and clustered into five groups using MOLPRINT2D fingerprints, Tanimoto similarity metrics and average cluster linkage method using Canvas (97). Whereas the decoys were selected from the ZINC database, using an in-house script that followed the Directory of useful decoys (DUD) methodology (97,98). All of these compounds were obtained from a previous paper (97), and they had previously been LigPreped using the OPLS2005 force field and generated one low energy ring conformation per ligand. The appropriate ionization states at pH 7.4 were assigned to all ligands. For the known PAMs and decoys, the chiral centers specified in literature were kept while unspecified centers were labelled racemic.

### 3.1.5 Receptor setup

The purpose of this step was to define the binding pocket on the receptor, and set up a receptor grid box which composes a set volume where the ligands are allowed to bind. The receptor gridbox was generated for each constructed homology model based on the agoPAM using the default settings:

- The docked ligand is confined to the enclosing box: centroid of the Workspace ligand (in this case the agoPAM)
- Size: Dock ligands similar in size to the Workspace ligand

The agoPAM was excluded from the receptor during the calculations of the receptor grid box, to make sure that it was not present in the later stages (during the docking).

### 3.1.6 Docking, scoring and model selection

Schrodinger's Glide SP docking procedure was performed on every model, to investigate the mode of binding in the pocket, and calculate the binding strength of the interactions between the ligands and the receptor. The default settings were used for this protocol: Scaling factor: 0.80, Partial charge cut-off: 0.15, flexible ligand sampling, sample nitrogen inversions, sample ring conformations, bias sampling of torsions for: All predefined functional groups, and add Epik state penalties to docking score (Glide SP and XP docking score, and the unit is given as kcal/mol).

The compounds were then ranked from good (low score) - bad (high score) based on Glide docking score. A large number of the decoys had better docking score than the PAMs, and some

of the PAMs had generally poor docking score. The binding pocket was therefore optimized further by using the induced fit protocol (using default settings), to 1) better the docking of the PAMs in the binding site, by generating an accurate complex structure for the ligand, and 2) to “rescue” the false negatives, in this case the PAMs that scored poorly. The PAM with the best docking score (for each model), was chosen as the compound to do the induced fit docking.

### **3.1.7 Induced fit docking**

Each receptor docking job had an output of 20 new receptor-ligand complex poses, and they were ranked based on their IFD score. Only the best model, for each of the receptors-ligand complexes, were picked for the rest of the experiments before the final model selection. A new set of receptor grid boxes were then generated based on the specific PAM in the complex, then there was a redocking of the PAMs and decoys in the newly generated binding pocket. Two of the PAM-clusters (cluster 3 and 4) were excluded from the redocking due to them binding in a non-satisfactory manner.

The compounds were ranked based on their docking score, and two of the models docked the PAMs with a good score, and at the same time filtered the highest amount of decoys, and they were selected as the final receptor-models to work with for the rest of the project.

### **3.1.8 Virtual screening of Molport and DrugBank**

#### **3.1.8.1 DrugBank**

The subsets of interest (approved, illicit, metabolites and withdrawn) were downloaded from the DrugBank website, and imported to Maestro. A ligand preparation step of the compounds was necessary. The compounds were prepared by using the default settings (except for “generate tautomers”): Force field: OPLS3e, Ionization: Generate possible states at target pH:  $7.3 \pm 0.1$ , Desalt, Computation: Retain specified chiralities (vary other chiral centers), and Generate at most 32 isomers per ligand.

The compounds were then docked into the four IFD-receptor models, where the models had their respective gridbox, using Glide SP docking protocol. The compounds were then ranked based on their docking score, and their docking orientation in the pocket. The compounds that had their docking pose occupying both the binding site and out towards the membrane/towards the extracellular loop region, were excluded from further investigation regardless of their docking score. Only the compounds with good docking score, and a binding orientation (mainly

positional) similar to the PAMs in the same binding site, were selected for the selection of hit compounds.

### 3.1.8.2 Molport

The Molport database (7,608,596 compounds) was downloaded from the website, and imported to Canvas. The physiochemical properties of the compounds were calculated, detailing the partition coefficient (log P), numbers of hydrogen bond donors and acceptors, number of rotatable bonds, molecular weight, and PSA (polar surface area). The compounds were then filtered based on Lipinski's Ro5, and Veber's flexibility principles. The Lipinski's Ro5 (rule of five) are a list of important physiochemical parameters used to evaluate druglikeness and determine if a drug molecule is likely to have a reasonable absorption characteristics and eliminates those that don't (99,100).

The rule states that for a drug to be orally active, it can't have more than one violation based on these parameters: no more than 5 HBD, no more than 10 HBA, a molecular mass less than 500 Da, and Log P coefficient that does not exceed 5 (101).

The Veber's flexibility principles are meant to complement the Lipinski's Ro5, as it is expected that molecules with large numbers of rotatable bonds and/or hydrogen bonds, would likely have molecular weights over 500 Da (102). The rules states that if the compound meets the criteria's of: a PSA not higher than 140 Å<sup>2</sup> and the molecule not having more than 10 rotatable bonds, are predicted to have good oral bioavailability (103).

A fingerprint was then calculated for each compound that passed the filtering step, using MOLPRINT2D (104). The reference PAM, TI-400, was then imported to the spreadsheet and the fingerprint was calculated using the same method. TI-400 was then used as a reference for the similarity screening on the database, and the compounds were grouped into bins based on their respective Tc value. The Tc value is a numerical measure of similarity ranging from 0-1, where 0 = no fingerprint overlap, and 1 = fingerprint identity (105). A visual inspection of the compounds in the different bins was performed and the compounds with a high Tc value and/or had similar features to TI-400 were selected for docking in Maestro. This resulted in 2.272 compounds from Canvas getting exported to Maestro, and prepared using the LigPrep protocol with same settings as mentioned earlier. The compounds were then SP docked into each of the four models, using their respective receptor grid box.

### 3.1.8.3 Final hit compounds selections

The potential hit compounds were selected from the models, using a last filtering method. This was necessary to reduce the number of compounds before purchase. The compounds from the DrugBank were selected by ranking the compounds based on their molecular weight and potential interactions with the nearby residues (after the docking), and the compounds with a molecular weight lower than 400 Da and promising interactions were selected. For the compounds from the Molport database, the compounds with the same/better docking score than TI-400 and similar binding pose orientation (positional and interactions with the nearby residues) were prioritized. Some QikProp properties were then calculated for each of the remaining compounds of interest to ensure that every compound had satisfactory ADME properties, before purchase. As a result of QikProp, the final number of 16 compounds were bought for in vitro experiment.

*Table 1 An overview of the QikProp descriptors used, and the details for each one of them. The information was obtained from the QikProp user manual (106)*

Descriptor	Explanation
#stars	<p>Number of property or descriptor values that fall outside the 95% range of similar values for known drugs. A large number of stars suggests that a molecule is less drug-like than molecules with few stars. Some of the following properties and descriptors are included in the determination of #stars: MW, dipole, PSA, donorHB, acptHB, QPlogPoct, QPlogPw, QPlogPo/w, logS, QPLogS.</p> <p>Range or recommended values: 0 – 5 stars</p>
#rtvFG	<p>Number of reactive functional groups. The presence of these groups can lead to false positives in screening assays and to decomposition, reactivity, or toxicity problems in vivo</p> <p>Range or recommended values: 0 – 2</p>
QPLogS	<p>Predicted aqueous solubility, log S. S in mol dm<sup>-3</sup> is the concentration of the solute in a saturated solution that is in equilibrium with the crystalline solid</p> <p>Range or recommended values: -6.5 – 0.5</p>

### 3.1.9 Part II: In Vitro

#### Materials

The materials used for the in vitro part was purchased from DiscoverX:

- cAMP Hunter™ CHO-K1 GABBR1+GABBR2 Gi Cell Line (Cat. #95-0165C2)
  - The CHO-K1 Wild Type (WT) cell line was provided by the Tumor biology research group of UiT, The Arctic University of Norway
- AssayComplete™ Revive CHO-K1 Media (Cat. #92-0016RM2S)
- AssayComplete™ CHO-K1 Cell Culture Kit 35 (Cat. #92-0018G2R2)
  - Components:
    - AssayComplete™ CHO-K1 Medium 35
    - AssayComplete™ Serum 35
    - AssayComplete™ Antibiotics Mix 35
- AssayComplete™ Cell Plating 2 Reagent (Cat. #93-0563R2A)
- AssayComplete™ Detachment Reagent (Cat. #92-0009)
- AssayComplete™ Preserve CHO-K1 Freezing Reagent (Cat. #92-0017FR2S)
- cAMP Antibody Reagent
- cAMP Detection Solution
- cAMP solution

This is the list of chemicals purchased from Sigma-Aldrich:

- CaCl<sub>2</sub> (Cat.# C7902)
- Ethanol (WM: 46.07), (Cat. #34923)
- HEPES (Cat.# H3375)
- MgCl<sub>2</sub>·6H<sub>2</sub>O (Cat.# M9272)
- KCl (Cat.# 746436)
- Trypan Blue 0.4 % Solution (Cat. #T8154)
- NaCl (Cat.# 746398)
- D-(+)-Glucose (Cat.# G7021)
- NaOH (Cat.# 30620)



- GABA (Cat.# A5835)
- DMSO (Cat.# 472301)
- Forskolin NKH477 (Cat.# N3290).

List over additional consumables and instruments used:

- Sterile PBS (Phosphate buffered saline)
- Liquid nitrogen
- Dry ice
- Countess® chamber slices
- Invitrogen Countess Automated Cell Counter
- MultiFlo™ FX Microplate Dispenser
- Clariostar Plus Microplate Reader
- Motorized pipette
- Cryogenic vials
- Pipettes (1, 2, 5, 10, 25 ml)
- Pipette tips (20, 200, 300, 1000 µL)
- Culture flasks (25, 75, 175 cm<sup>2</sup>, Millicell® HY 5 layer)
- Centrifuge tubes (15, 50 ml)
- Eppendorf tubes (1, 2, 5 ml)
- Eppendorf Flat Cap Strips (8 strips)

The test compounds used were purchased from Molport.

## Method

### 3.1.9.1 Buffer preparation

The buffer preparation step was necessary, as it was needed to make stock solutions of the test compounds, run assays, harvest cells, and as a solvent for the solubility test of the compounds. Four stock solutions (the constituents are listed in table found below) were mixed together to make a big batch of 20xHBSS (Hank's balanced salt solution) buffer.

*Table 2 An overview over the constituents/ingredients which makes up the four different stock solutions used to make the 20xHBSS buffer.*

Stock solution	Chemical compound/constituents	Molarity pr. 100 ml
Stock 1	NaCl	2.630 M (2630 mM)
	D-glucose	0.2 M (200 mM)
	KCl	0.1 M (100 mM)
Stock 2	CaCl <sub>2</sub>	0.027 M (27 mM)
Stock 3	MgCl <sub>2</sub> * 6H <sub>2</sub> O	0.020 M (20 mM)
Stock 4	HEPES	0.2 M (200 mM)

A portion of this buffer was then diluted ten times to make a 2xHBSS buffer, which was used for the solubility test of the compounds and run the different assays. The 2xHBSS buffer was prepared by making a 400 ml stock. This process was made by mixing equal amounts of the four stock solutions, adding the desired double distilled water (ddH<sub>2</sub>O), and sodium hydroxide (NaOH) to adjust the pH to emulate the physiological environment in the body. 1xHBSS buffer (also referred to as assay buffer) was prepared by mixing the same amount of ddH<sub>2</sub>O and 2xHBSS buffer, and the osmolarity was measured to ensure that the desired concentration/osmolarity was obtained. The 1xHBSS buffer was then stored in the refrigerator for later use.

### **3.1.9.2 Test compound preparation and solubility test**

The test compounds were dissolved in 100% DMSO to make stocks of 10 and 20mM, and allocated into cryovials for storage at -20°C in the freezer. The solubility test was performed by mixing a portion of the test compound stock with 2xHBSS buffer, at a concentration of 60 µM. Every test compound, except for two, seemed to be stable at this concentration, not making any crystals. The ones that failed the test, were prepared in a lower concentration of 30 µM, to see if it was possible to obtain a stable solution without the formation of crystals. One of the two compounds passed the test under these conditions, while the last compound had to be prepared in 5mM D-glucose (5G) solution at a concentration of 60 µM. This step was important, as it was used to determine the optimal final concentrations of the test compounds in the assay; the concentrations being 10 µM (for the test compounds that passed the solubility at 60 mM 2xHBSS buffer/5G) and 5 µM (for the test compounds that passed the test at 30 mM 2xHBSS buffer).

### **3.1.9.3 Cell culturing and harvesting of cells for assay**

The cell culture step was split into three phases; cell seeding, cell splitting and cell harvesting. The two first steps were done with ultimate precision, under sterile conditions to ensure that a high quality of the cells would be used for the assays, while the cell harvesting had less focus on the sterile part. This will be explained further in the discussion.

The cell seeding procedure was performed by thawing cryovials with either GABA<sub>B</sub> / WT-cells, stored in a liquid nitrogen tank, using a water bath at 37°C, until a small ice crystal was left in the vial. This vial was quickly transferred to the fume hood, where it got suspended with 10 ml of preheated culture media into a 15 ml conical tube. The suspension then got centrifuged at 350 G for 4.5 minutes, and a cell pellet was formed at the bottom. The liquid phase was then aspirated from the tube, leaving just the cell pellet, which got re-suspended with 11 ml of preheated culture media. The cells were then seeded into two T25 flask, each with 5 ml cell suspension and stored in an incubator for growth, at 37°C and 5% CO<sub>2</sub> for 48 hours (or 36 hours for the WT-cells) and these settings were kept throughout the in vitro portion.

The cell splitting was performed after 48 (or 36) hours, when the cells had reached the desired confluency at 75-80%. The culture media was aspirated from the T25 flask, and the flasks got rinsed with 15 ml of preheated PBS, 5 ml at a time with continuous liquid aspiration. 1 ml of detachment reagent was added to the flasks, to detach cells from the surface, and the flasks

were stored in the incubator for 2 minutes with the same settings mentioned earlier. A check of the T25 flasks under a microscope was performed, as it was important to confirm that the cells were detached from the inner surface of the flasks. The cells were then harvested with 15 ml of preheated PBS and transferred into a 50 ml conical tube before centrifuging at 350 G for 4.5 minutes. The liquid phase was aspirated, and the cell pellet was re-suspended with 16 ml of preheated culture media. The cell suspension was then seeded into a T75 flask, and stored in the incubator for continuous growth. This passage of cells was performed when the cells reached around 75% confluency. The first part of this seeding step was the same as the seeding of T75 flask with a few differences: the T75 was rinsed with 30 ml of preheated PBS (using 10 ml at a time), and the cells were detached using 2 ml of detachment reagent. After the aspiration of the liquid phase of the cell suspension, the cell pellet was re-suspended with 10 ml of preheated culture media. A small sample of this cell suspension was then transferred into an Eppendorf tube, and carried to a cell counter to determine the cell density and viability, as this was an important step before seeding the cells into a T75 and T175 flask. 50  $\mu$ L of cell suspension was mixed with 50  $\mu$ L of trypan blue, and 20  $\mu$ L of this mixture was loaded into two Countess® chamber slices for counting using Countess® automated cell counter. The cell concentration was then diluted, and the desired amount of cells (1.5 million cells for T75 and 3.5 million cells for T175) were seeded into the culture flasks and stored in the incubator for continuous growth.

The procedure for the cell harvesting on the day of the assay, was performed as aforementioned, with a few differences; the cells were detached using 3 ml of detachment reagent, the cell suspension was centrifuged twice (first time with 30 ml PBS being the liquid phase, and the second time with 40 ml of assay buffer), and the final cell harvesting after liquid aspiration, was done by using 15 ml assay buffer. The cell suspension was then brought to the cell counter (the same procedure as described earlier) and diluted to a concentration of 0.8 million cells/ml, given that the desired amount of cells (between 18-20 million) and viability (>96%) was obtained. The cell suspension was then put for incubation on a water bath at room temperature, for 2 ½ hours.

### 3.1.9.4 Assay preparation and embodiment

The assay preparation was performed in different manners, based on the assay ran on the actual day. The final assay concentration of both GABA and forskolin, was predetermined to be 30  $\mu\text{M}$  (in all of the assays where one or both of these components were involved).

**Time dependent cAMP assay:** The objective of this assay was to determine the best reaction time, by finding an assay window where the reaction (for the planned GABA<sub>B</sub>/WT assays) would generate almost the same results regardless of the reaction time as long as it was within the assay window. Forskolin was diluted with ddH<sub>2</sub>O to a concentration of 180  $\mu\text{M}$ , from a stock of 5 mM, and mixed with 2xHBSS in a ratio of 1:1. 5  $\mu\text{L}$  of this mixture was then applied to 48 wells on a 384-well microplate (using a 8 channel pipette) minutes before the incubation time for the cells passed. 10  $\mu\text{L}$  of the cells were quickly dispensed to the microplate (in the same wells as the forskolin-2xHBSS mix) using a MultiFlot™ FX Microplate Dispenser and quickly moved to the Clariostar Plus Microplate Reader. With the microplate reader, cAMP solution and antibody were added to the microplate at predetermined time points. The cAMP detection solution was added to the microplate after 1-hour reaction time, following the same time points. The results were then read twice after 14-16 hours.

**Forskolin dependent cAMP assay:** The objective of this assay was to try and explain why the final assay concentration of forskolin (at 30  $\mu\text{L}$ ) was desired.

**GABA dose response cAMP assay (without test compounds):** The objective of this assay was to determine the amount of cAMP the GABA<sub>B</sub> cells would produce being stimulated by forskolin, while GABA was present in the mixture. GABA was prepared by weighing a certain amount of powder, and mixed with ddH<sub>2</sub>O to make a stock solution with the concentration of 40 mM. The stock was then diluted to 240  $\mu\text{M}$  with ddH<sub>2</sub>O, and this newly made stock was further diluted 11 more times with ddH<sub>2</sub>O (1 ml stock and 2 ml ddH<sub>2</sub>O) where 8 of the 12 dilutions were picked for the assay.

Forskolin was prepared the same way as mentioned earlier; albeit with a concentration of 360  $\mu\text{M}$  instead of 180  $\mu\text{M}$ . Forskolin and GABA was mixed in the ratio of 1:1 in Eppendorf Flat Cap Strips (8 strips) using a 8 channel pipette. This mixture was then mixed 1:1 with 2xHBSS buffer in a new set of Eppendorf strips and 5  $\mu\text{L}$  of this new mixture was loaded into 48 wells on a 384-well microplate (minutes before the cell's incubation time was over) using the

appropriate pipette. The cells were then dispensed to the microplate and quickly transferred to the microplate reader, where it was incubated for 24 minutes (reaction time). The cAMP solution and cAMP antibody were loaded onto the microplate, and then the cAMP detection solution after 1 hour reactions time. The results were read twice after 14-16 hours.

**WT cAMP assay:** The WT cAMP assay was run to see if some of the test compounds had an effect on the cAMP produced by the forskolin. This assay was prepared the same way as aforementioned. Only difference is that the test compounds were included in the mix. The test compounds with stock concentration 20  $\mu\text{M}$ , were diluted to 10  $\mu\text{M}$  in DMSO. Two sets of forskolin mixes were made: the forskolin-2xHBSS mix and the forskolin-ddH<sub>2</sub>O mix. The forskolin-2xHBSS mix was used for the compounds that were solved in either 5G or NaOH, and the forskolin-ddH<sub>2</sub>O mix was used for the compounds that passed the solubility test in 2xHBSS buffer. The rest of the assay was carried out the same way as the GABA dose response assay.

**EC<sub>20</sub>/EC<sub>80</sub> cAMP assay:** This assay was prepared and run the same way as the GABA dose response cAMP assay, with the only real differences being that the test compounds were included and only to GABA concentrations were picked.

## 4 Results

### Part I: In Silico

#### **Homology modelling:**

The model evaluation step was done by reviewing the Ramachandran plot as shown in the figures below. The plot shows that the majority of the amino acids are located in the allowed region. Results are only shown for the models that were picked for the drug screening.

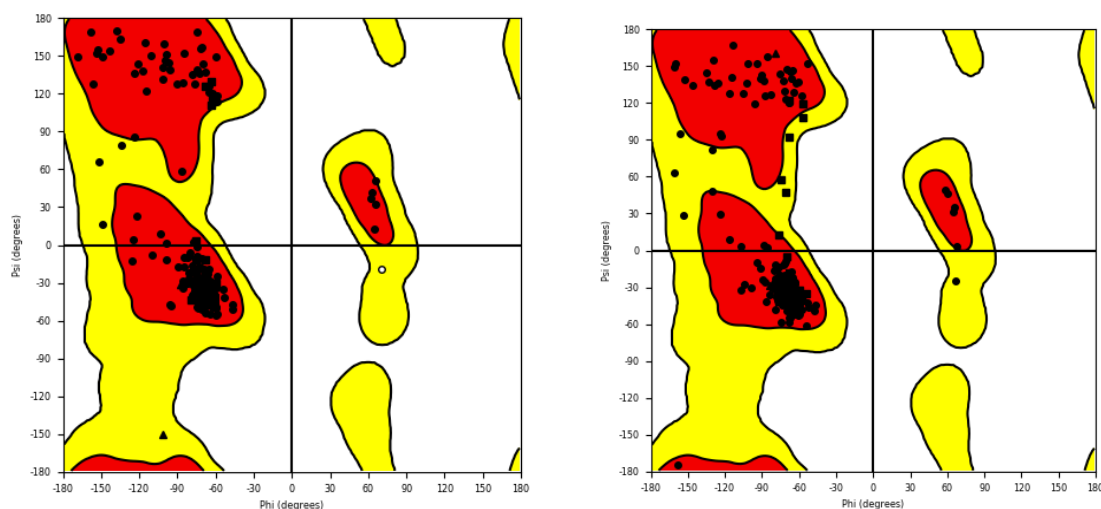


*Figure 8 The Ramachandran plots for a) model 1 and b) model 3. These models show the placement of the amino acids in the regions. The white region corresponds to the “forbidden zone”, red regions corresponds to the allowed region and the yellow regions corresponds to the additional allowed region.*

#### **Model selection:**

The results from the docking done for the model selection, are represented in the tables below.

*Table 3: The docking results of the PAMs in receptor model 1 before and after IFD. The docking results for the PAM clusters 3 and 4 are not included in the table due to their non-satisfactory binding mode (as mentioned in the method)*

PAM cluster	Glide Docking Score Range, Before IFD	Glide Docking Score Range, After IFD
1	(-4.164 - -6.050)	(-5.998 - -7.636)
2	(-6.139 - -7.278)	(-5.678 - -9.468)
3	(-4.384 - -7.252)	
4	(-5.223 - -7.963)	
5	(-3.636 - -5.731)	(-6.332 - -7.681)

*Table 4: The docking results of the PAMs in receptor model 2 before and after IFD. The docking results for the PAM clusters 3 and 4 are not included in the table due to their non-satisfactory binding mode (as mentioned in the method)*

PAM cluster	Glide SP Docking Score Range, Before IFD	Glide SP Docking Score Range, After IFD
1	(-3.710 - -4.768)	(-5.900 - -6.802)
2	(-3.763 - -5.279)	(-6.980 - -8.265)
3	(-3.695 - -4.889)	
4	(-4.056 - -5.978)	
5	(-4.585 - -5.495)	(-6.771 - -8.266)



*Table 5: The docking results of the PAMs in receptor model 3 before and after IFD. The docking results for the PAM clusters 3 and 4 are not included in the table due to their non-satisfactory binding mode (as mentioned in the method)*

PAM cluster	Glide SP Docking Score Range, Before IFD	Glide SP Docking Score Range, After IFD
1	(-4.660 - -5.962)	(-5.900 - -7.632)
2	(-4.792 - -7.192)	(-8.820 - -10.497)
3	(-4.291 - -6.273)	
4	(-5.712 - -8.438)	
5	(-5.701 - -6.520)	(-7.290 - -10.016)

*Table 6: The docking results of the PAMs in receptor model 4 before and after IFD. The docking results for the PAM clusters 3 and 4 are not included in the table due to their non-satisfactory binding mode (as mentioned in the method)*

PAM cluster	Glide SP Docking Score Range, Before IFD	Glide SP Docking Score Range, After IFD
1	(-4.077 - -5.518)	(-3.905 - -5.938)
2	(-6.561 - -7.395)	(-4.131 - -6.367)
3	(-5.230 - -6.174)	
4	(-5.412 - -7.182)	
5	(-4.600 - -7.141)	(-4.467 - -5.460)

Based on these results, model 1 and 3 were picked for the rest of the project.

#### Virtual screening of the DrugBank and Molport databases

##### Database filtering:

The Molport database was downloaded, and 7.608.596 compounds were filtered using a multistep approach, with different types of filtering protocols as shown in the figure below. The output after the filtering steps, were exported to Schrödinger Maestro.

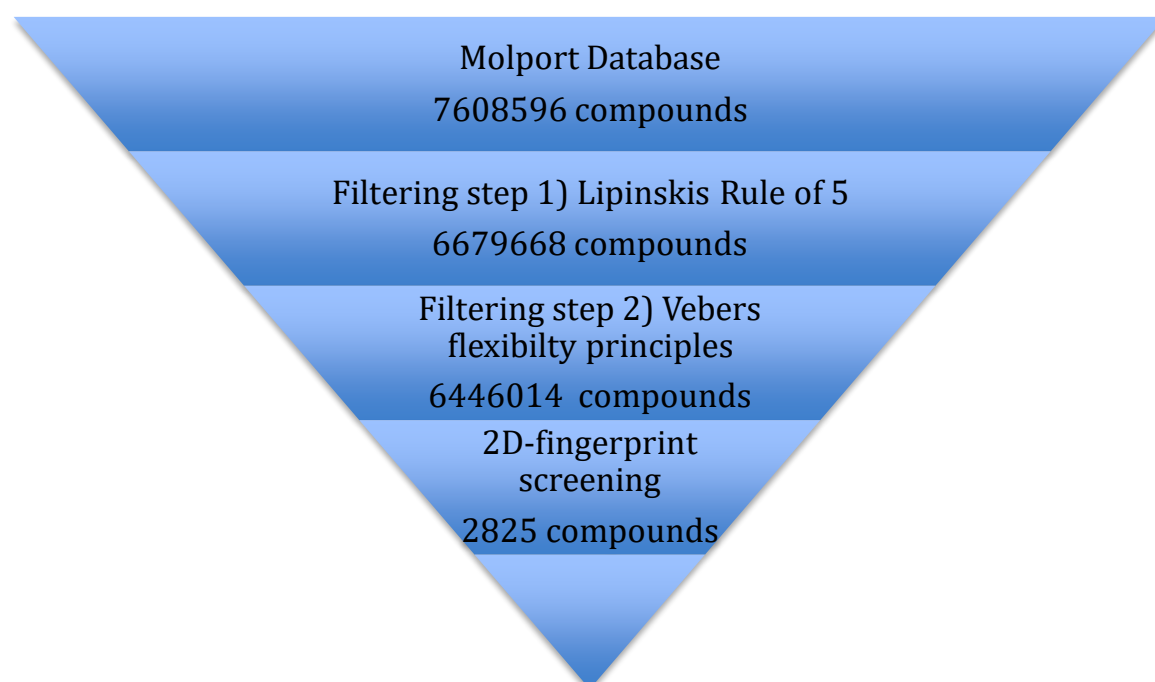


*Figure 9 Multistep virtual screening results. The figure shows the number of compounds after each filtering step.*

In order to perform the 2D-fingerprint based screening, the reference GABA<sub>B</sub> PAM TI-400 was selected. The screening was done by using the binary fingerprint (hashed) on the dataset, and the cut-off value were determined by screening the reference ligand with the same fingerprint.

##### Purchase of test compounds:

The compounds of interest (found in the table below) after the docking procedure, were bought based on the availability, price and the QikProp calculations.

Table 7 The results from the screening of the Molport database. The table shows the analogues bought based on the reference PAM TI-400

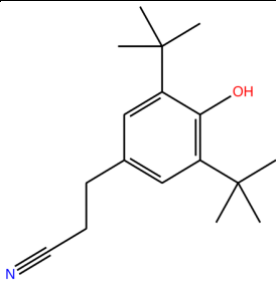
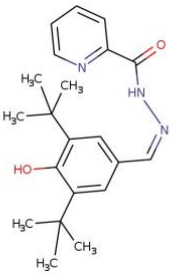
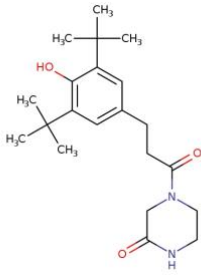
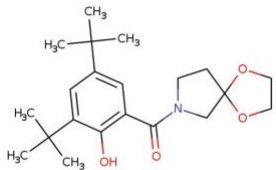
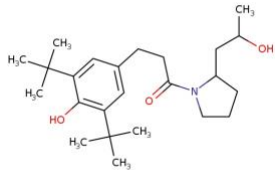
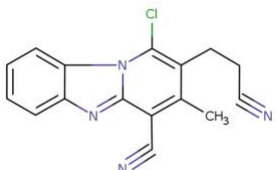
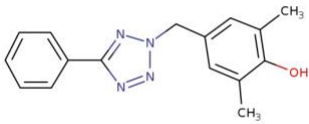
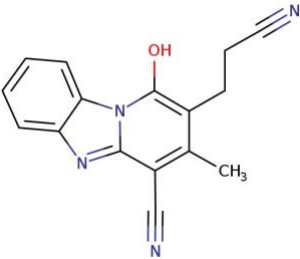
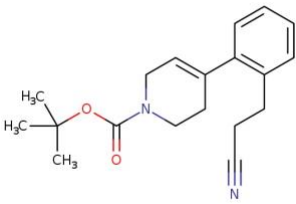
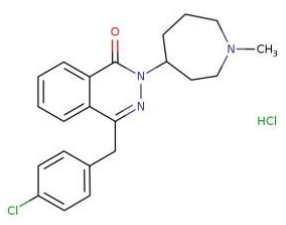
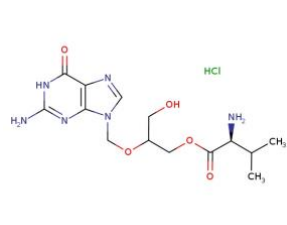
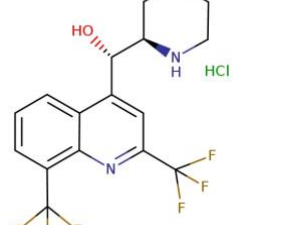
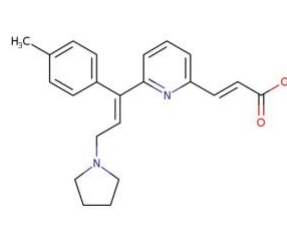
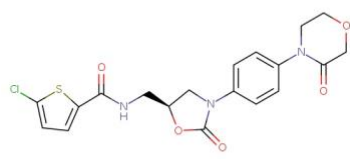
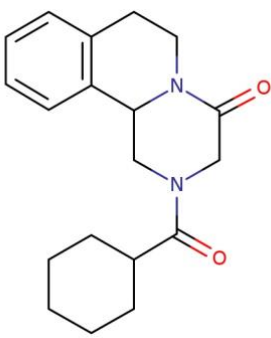


 <p>Reference PAM TI-400</p> <p>SP Docking score: -7.825 kcal/mol</p>	 <p>Compound I-7</p> <p>SP Docking score: -8.737 kcal/mol</p>	 <p>Compound I-12</p> <p>SP Docking score: -9.377 kcal/mol</p>
 <p>Compound I-15</p> <p>SP Docking score: -9.253 kcal/mol</p>	 <p>Compound I-16</p> <p>SP Docking score: -9.203 kcal/mol</p>	 <p>Compound I-23</p> <p>SP Docking score: -8.707 kcal/mol</p>
 <p>Compound I-24</p> <p>SP Docking score: -8.790 kcal/mol</p>	 <p>Compound I-25</p> <p>SP Docking score: -9.235 kcal/mol</p>	 <p>Compound I-27</p> <p>SP Docking score: -9.478 kcal/mol</p>

Table 8 The results from the screening of the DrugBank database

 <p>Compound I-2</p> <p>Docking score: -10.093 kcal/mol</p>	 <p>Compound I-3</p> <p>Docking score: -9.319 kcal/mol</p>	 <p>Compound I-4</p> <p>Docking score: -9.426 kcal/mol</p>	 <p>Compound I-5</p> <p>Docking score: -9.695 kcal/mol</p>
 <p>Compound I-10</p> <p>Docking score: -9.876 kcal/mol</p>	 <p>Compound I-30</p> <p>Docking score: -9.321 kcal/mol</p>	 <p>Compound I-31</p> <p>Docking score: -8.894 kcal/mol</p>	 <p>Compound I-32</p> <p>Docking score: -9.308 kcal/mol</p>

## Part II: In Vitro

### Time-dependent cAMP assay:

From the results, it is shown that the cells reached a maximum stimulation (between 7000 and 8000 relative light units) after 24 minutes and it was stable for three more minutes before a small increase in the RLU (relative light units). This gives us a 3-minute assay window, where we are able to stop the reaction (between GABA/WT, forskolin and the cells as mentioned in the methods) by dispensing cAMP reagent.

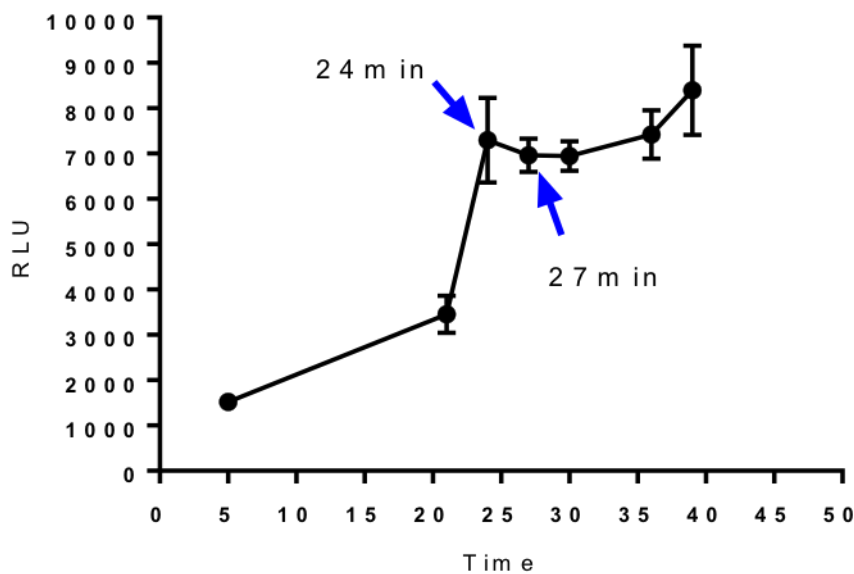


*Figure 10 This figure represents the results obtained from running the forskolin time-dependent assay. The reaction was run at 25 °C. The GABA cells were incubated for 2 ½ hours on water bath at 25 °C, prior to the reaction. The numbers on the x-axis represents the time points used for the reaction, while the y-axis represent the relative light unit (the unit of measure for ATP.)*

Forskolin dose response cAMP assay:

The results from this experiment, shows that we got an forskolin EC<sub>50</sub> (effective concentration) = 3.53 μM which is a similar to what the manufacturers got, running the same assay (3.2 uM).

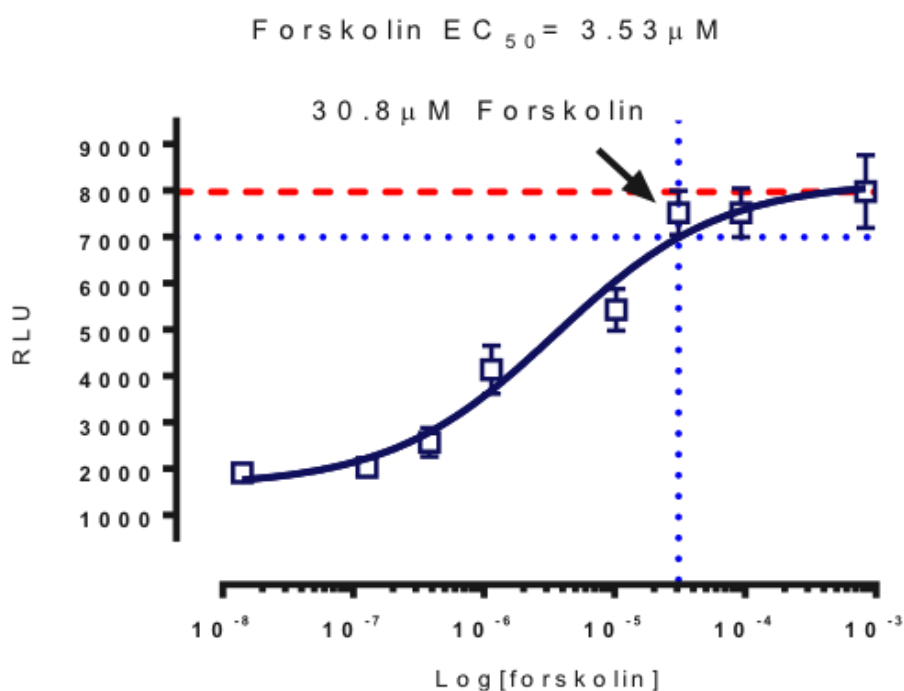


*Figure 11 Forskolin dose-response on GABA cells. The reaction was run at 25 °C. The GABA cells were incubated for 2 ½ hours on water bath at 25 °C, prior to the reaction. The numbers on the x-axis represents the concentration of forskolin used for the reaction, while the y-axis represent the relative light unit.*

GABA dose response without test compounds:

This experiment was repeated three times, and the average RLU of each GABA concentration was used to make a graph, and calculate the EC<sub>50</sub>. The EC<sub>50</sub> obtained from this assay was 164 nM. From this the EC<sub>20</sub> and EC<sub>80</sub> were determined.

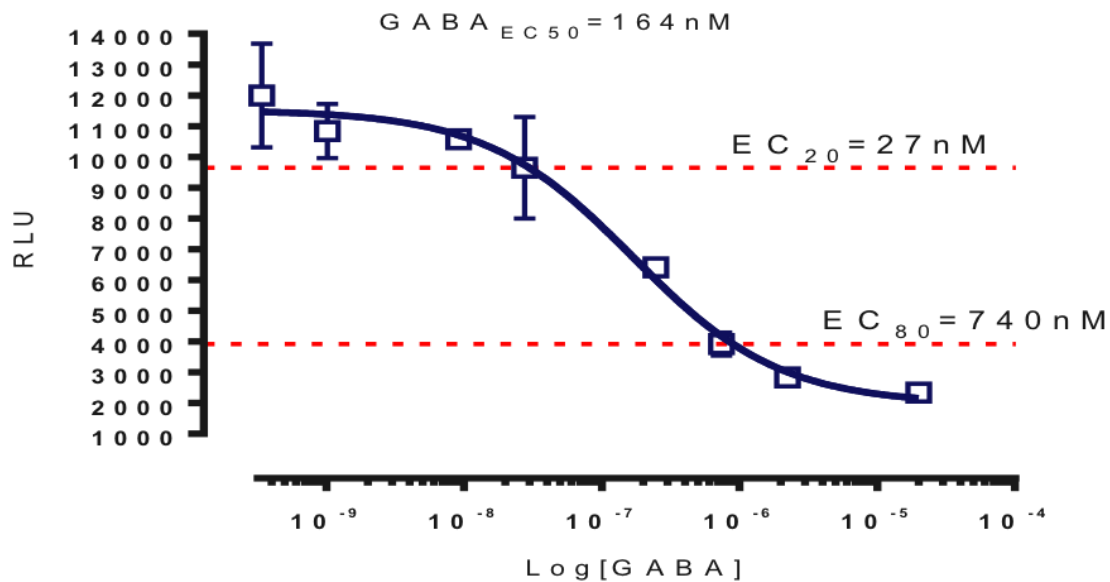


Figure 12 GABA dose-response on GABA cells. The reaction was run at 25 °C. The GABA cells were incubated for 2 ½ hours on water bath at 25 °C, prior to the reaction. The numbers on the x-axis represents the concentration of GABA used for the reaction, while the y-axis represent the relative light unit.

#### WT cAMP assay

The experiment was repeated three times, to make sure the results were accurate. The results show the compounds and their presumed effect on the WT cells, in the presence of just forskolin. A threshold of +/- 10 percent of the RLU values for the controls, was used as the cut-off. Every compound that fell outside of this threshold, were removed. Since the WT cells doesn't express any GABA receptors, all of the compounds with lower RLU than the controls were removed since it indicates that the mechanism of action doesn't go through GABA (results not shown).

#### EC<sub>20</sub> & EC<sub>80</sub> cAMP assay:

The results show the effect of the test compounds, in the presence of GABA in different concentrations ( $EC_{20} = 27 \text{ nM}$  and  $EC_{80} = 740 \text{ nM}$ ), using GABA cells. This experiment was repeated twice, to make sure the results were accurate. Unlike the WT cAMP assay, the compounds that reduced the RLU (compared to the controls) were selected for further investigation, as this could indicate that the compounds (I4, I7, I23 and I24) work through the  $GABA_B$  receptor. Compound I10 was also picked for further investigation, as it was difficult to understand the effect it had on the GABA cells.

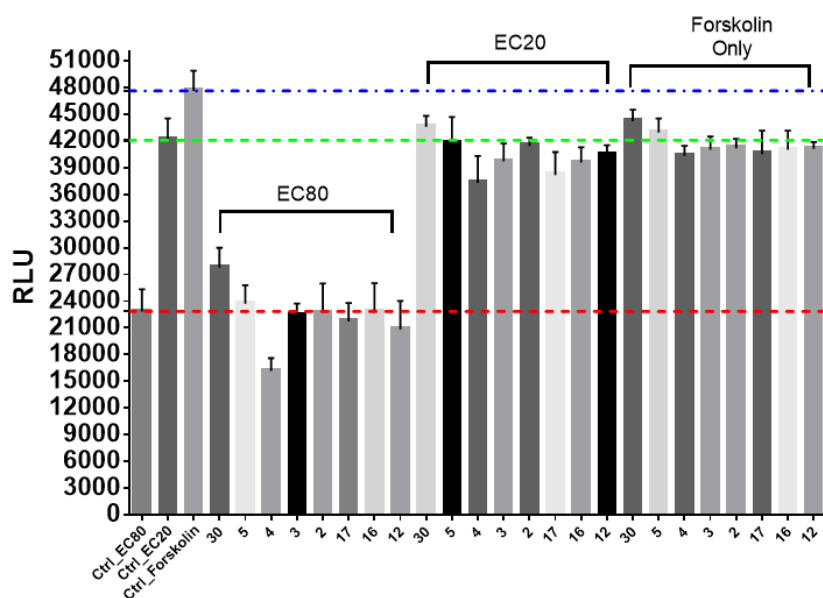


Figure 13: Functional  $EC_{20}/EC_{80}$  cAMP assay. The reaction was run at  $25 \text{ }^\circ\text{C}$ . The GABA cells were incubated for  $2 \frac{1}{2}$  hours on water bath at  $25 \text{ }^\circ\text{C}$ , prior to the reaction. The numbers on the x-axis each represents the test compounds used for the reaction, while the y-axis represent the relative light unit. The comparison between compound I4 and the controls, indicates mechanism through  $GABA_B$  receptor.



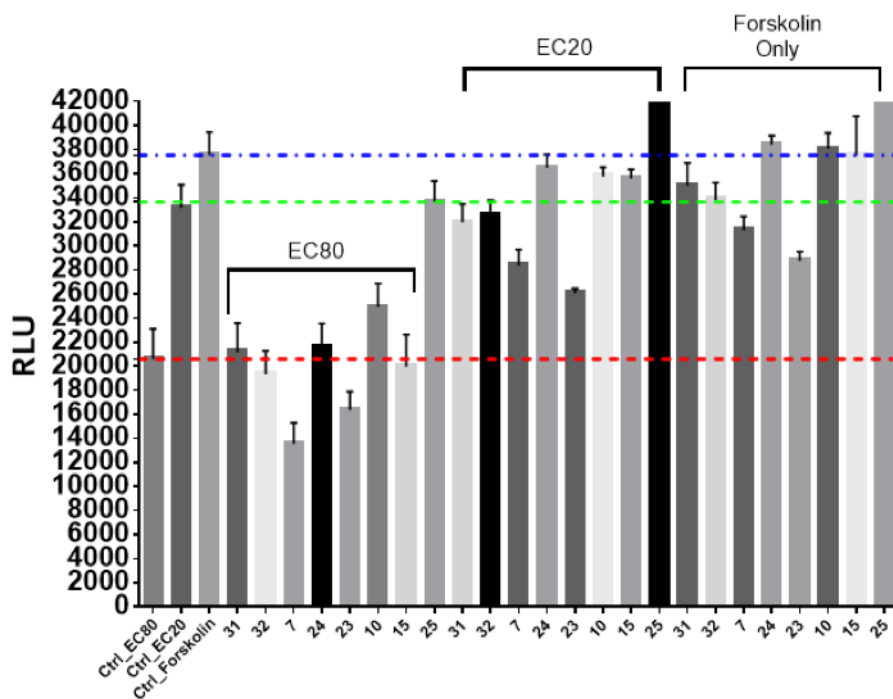


Figure 14: EC20/EC80 cAMP assay. The reaction was run at 25 °C. The GABA cells were incubated for 2 ½ hours on water bath at 25 °C, prior to the reaction. The numbers on the x-axis each represents the test compounds used for the reaction, while the y-axis represent the relative light unit. The comparison between compounds I7, I10, I23, I24 and the controls, might indicate mechanism through GABA.

GABA dose response with test compounds:

The results from the last phase of in vitro testing, shows us the effect of the promising compounds; I-4 and I-10 in the presence of GABA. From the curve, it seems like compound I-4 reduces the  $GABA_{EC50}$  from 294 nM to 78 nM indicating that it might be a PAM, although a weak one since it doesn't seem to reduce the GABA concentration by much. Looking at compound I-10, it seems like this compound increases the  $GABA_{EC50}$  from 294 nM to 442 nM indicating that it may be either an antagonist or NAM, and we see a slight increase in the GABA concentration.

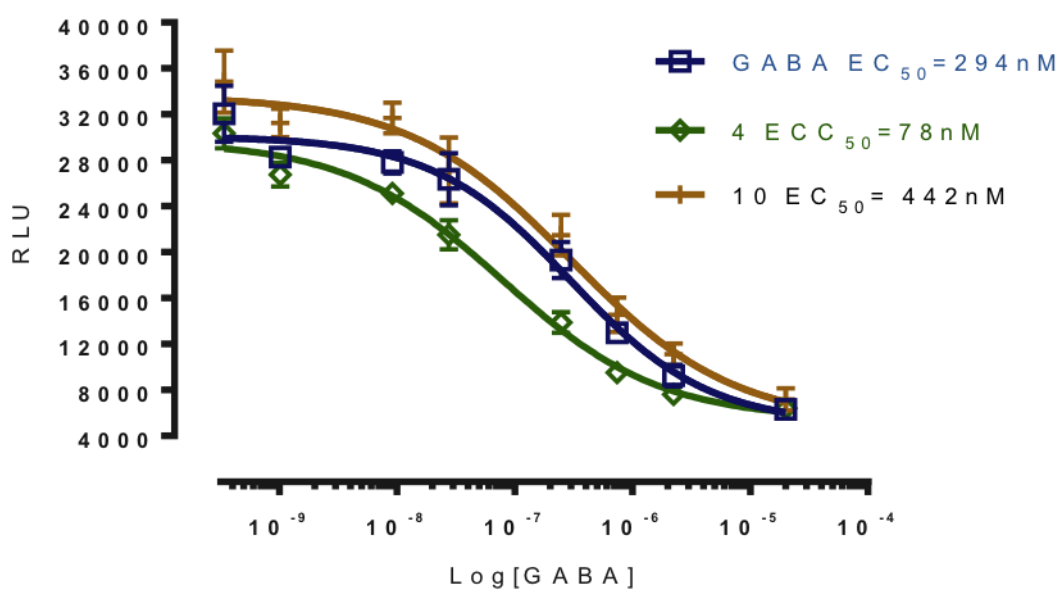


Figure 15 Test compounds with the presence of GABA. The reaction was run at 25 °C. The GABA cells were incubated for 2 ½ hours on water bath at 25 °C, prior to the reaction. The numbers on the x-axis represents the concentration of GABA used for the reaction, while the y-axis represent the relative light unit.

## 5 Discussion

The aim of the study was to try and find new allosteric modulators, especially PAMs for the GABA<sub>B</sub>-receptor. This was done by using methods within computational chemistry and experimental lab. The combination of both approaches gave us the opportunity to find new candidates, and investigate the mode of action of said compounds.

### Part I: In Silico

#### Virtual screening approaches

For this part of the project, both SBVS (structure based virtual screening) and LBVS (ligand based virtual screening) approaches were used. The Molport database was primarily screened by using the LBVS approach. MOLPRINT2D was the technique used as previous studies (85,107) has mentioned that this technique is the best to use if you're uncertain about the right fingerprint type for your set of ligands (85,107). At the same time, they also recommend using multiple fingerprint types as not all of them are ideal for the active compounds. We could've tried this approach if we'd have more time, but because of the complexity of the project we decided to use MOLPRINT2D.

The similarity cut off value, was decided by looking at the compounds manually. Had we picked compounds strictly based on the Tc value, the number of compounds to be docked using the SBVS approach would be minimal. What we found out from using this approach, is that many of the compounds were similar to the reference structure, but often got a critically low value if there were some difference (for example: having one less methyl group in the structure). This would maybe not be the case if we use different fingerprint types as they use criterion.

The SBVS approach, included the docking of the test compounds into the defined binding site. The Glide SP docking protocol was preferred, due to the huge number of compounds we decided to dock into each receptor model. Although Glide XP docking is believed to be more accurate than SP docking, it's not recommended for a huge set of compounds as it is time-consuming.

Another issue includes the use of the semi-rigid docking. As we now from countless studies, the receptors in our body are in constant motion. The binding of an active compound will cause a conformational change in the receptor, but this is not seen with the docking protocol we've used. Usually, a standard docking protocol only involves one structure to represent the receptor, overlooking the changes in the binding pocket geometry induced by ligand binding (108). Different ligands may stabilize different receptor conformations with different internal cavities (108). Therefore, by using this semi-rigid docking, we could introduce many false negatives and identify less diverse compounds (109). Therefore, a more useful approach for the future, would be to utilize a flexible docking protocol.

Fortunately, we were able to overcome some of the problems, by screening from the DrugBank. This gave us the opportunity to find diverse structures, instead of just looking for analogues of our reference PAM.

### Homology modelling

As of today, only the extracellular domain of the GABA<sub>B</sub>-receptor is crystallized. This is the reason for why we had to build theoretical 3D-structures of the receptor. The models built for the docking process, were based on the active-like receptor structure of mGlu1 (manuscript in preparation). The models were validated by looking for hallmarks mentioned in the literature. The first thing we looked for was the “ionic lock”, which is referred to as a molecular switch that keeps the GPCRs in an inactive state (42). This interaction is seen between Lys678 (in helix 3) and Glu783-based on the mGlu1 residue numbering (in helix 6) (110), and this was also observed in all of the built models. The next we looked at was the disulphide bond which is conserved through all GPCR classes. This interaction is found between the extracellular loop 2 (Cys657) and extracellular loop 3 (Cys746) (42). This interaction was also found in our models, so we went on to use them for the docking of the compounds.

The model evaluation included the Ramachandran plot, and the docking of the decoys and PAMs. The Ramachandran plots (figure 8) showed that the built models were of good stereochemical quality, since all of the amino acids were located in the allowed sections meaning that they wouldn't cause any problems in the helices or the b-sheets.

The receptor gridbox for each model, was based of the agoPAM's position in the model. This may have caused a bias in the docking mode of the compounds, as the allosteric binding sites are less conserved across the different classes of GPCRs (110). The best approach would most

likely be to choose important residues in the GABA<sub>B</sub>-allosteric binding site (that are known to participate in the ligand-receptor interactions) based on the GABA<sub>B</sub>-receptor site-directed mutagenesis study (63). The point mutation study showed that by mutating Gly706 GABA with Tyr, and Ala708 with Pro, they were able to activate the transmembrane domain using GS39783 in the absence of GABA (63). And for this reason, we could've achieved a more accurate docking of the compounds.

Docking of the decoys and the PAMs, didn't provide any clear answers regarding to if the models were of good quality or not. The models we built, bound almost every decoy we docked and this made it raised questions about the models. The reason being that the decoys in theory are not supposed to bind to the binding, although the physiochemical properties may be similar to the known binders.

Due to the lack of experimentally testing of the decoys, we have not been able to actually determine if the selected set of compounds don't bind to the receptor. Because of this, we were forced to visual inspect the docking pose of the decoys in the binding pocket. What we saw was the decoys had a tendency to occupy multiple spaces: the binding pocket, up towards the extracellular loops and out towards the membrane. One other reason might be that the constructed models had huge spaces between the helices, which in turn allowed for the docking outside of the desired binding site.

The PAMs on the other hand, only docked inside the determined active site. And for this reason, the best scoring PAM from the best PAM cluster (in regards to docking score and binding mode), was selected to the induced fit docking. This resulted in many of the decoys not binding to the receptor, since the new receptor grid box now was based on the specific PAMs and not the agoPAM from before.

#### Comparing the inactive GABA<sub>B</sub> structure to the active structure

The inactive structure of the GABA<sub>B</sub>-receptor (homology model) was obtained from a previous study (97). The two structures were superimposed on to each other based on the C $\alpha$ -carbons, to display the key differences between the two models. The active structure shows that the TM3, TM5 and TM6 form a pore-like structure (an open binding site), compared to the inactive structure where the TMs are organized tightly. One thing the models share in common, is the ionic lock. This indicates that the "active-like" conformation of the receptor is not all the way active, but more so in an intermediate state.

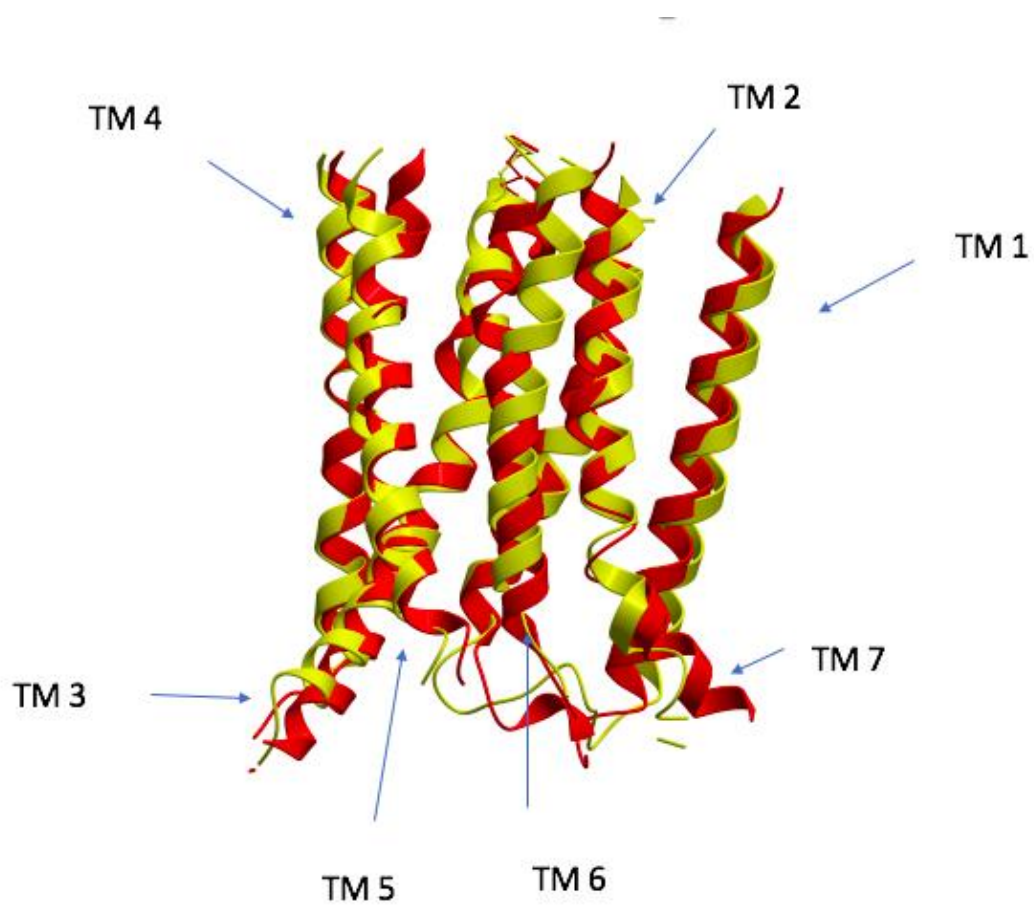


*Figure 16 Superimposition of the active and inactive GABA<sub>B</sub> receptor shown as ribbons. The yellow ribbons represent the active conformation, whereas the red ribbons represents the inactive structure. Figure made using ICM. RMSD value = 0.9 Å.*

## Part II: In Vitro

This part of the project was done to investigate the effects the compounds could mediate through the GABA<sub>B</sub>-receptor, the regulation of cAMP to be more specific. This was done by running multiple cAMP assays, to assess if we had compounds with PAM/agonist or NAM/antagonist effect. It took time to set up the right protocols, especially getting the correct amount of cells, the right buffer concentration (osmolarity), having the right assay condition, finding the right concentration to solubilize the test compounds, doing extensive training to make sure we could validate our method etc.

We experienced a lot of problems replicating the results, doing the different assays. Working with the cells, we experienced that the cell cycle mattered as they determined the amount and the quality of the cells. It took five days from cell seeding to we could run an assay, only if the desired number of cells were reached. The cell cycle for the WT-cells is 36 hours, so whenever we started the cell seeding, we weren't able to escape working during the night which caused some inaccuracies with the protocols. At some point we had to coordinate the seeding of both WT and GABA cells which, but it was worth it as we got rewarded by finding new potential allosteric modulators.

We also used a cheaper version of the culture medium, due to it being almost as effective as the original one from the manufacturers. Cell internalization was one important thing we had to keep in mind as this process would make the surface receptors go back into the cell, meaning that the amount of cAMP mediated through the receptors would be reduced and affect our results. Therefore, we had to be careful with how we handled the cells in the conical tubes, the temperature we exposed them for and the reaction time as all of the factors could affect the cAMP signal.

### Forskolin-concentration dependent cAMP assay

This assay was performed, so we could determine the final concentration of forskolin in the assay. The reason for why the EC<sub>80</sub> was selected and not the other concentration, is because a lower EC may give us an increased number in false negative and false positive results. Using the maximum EC wouldn't be expedient as we wouldn't be able to detect an increase in the RLU, by the test compounds.

### EC<sub>20</sub> and EC<sub>80</sub> cAMP assay

These concentration was retrieved from the manufacturers, as a guide for the cell line bought from them. This assay was used to weed out the test compounds that seemed to have either increasing or decreasing effect on the cAMP production with the presence of GABA in the predetermined concentrations. The compounds that seemed to have an effect on the cAMP, were further investigated with a WT cAMP assay. The reason being that the WT-cells themselves don't have any GABA that could reduce the cAMP, so a change in response indicates that the mechanism is carried out by other receptors, and not necessarily GABA<sub>B</sub>. From this method of testing, four compounds seemed to have very interesting results.

### Ligand-receptor interactions:

However, with the flaws of the methods used, we still were able to find four hits – two from Molport and the rest from DrugBank. Especially the compounds from DrugBank are of interest, as they provide us with the opportunity to investigate the function of the drugs in GABA signaling. Drug repurposing is, as mentioned before, a super useful in the drug discovery, as it can shorten the time it takes do find new therapeutic agents. The drugs have already been through all of the clinical testing, and most of the adverse effects have been found but not all of them have been understood.

The hits we got from the DrugBank are: Mefloquine (I-4) and Rivaroxaban (I-10), where Mefloquine was found to be a weak PAM, and Rivaroxaban was a NAM. Mefloquine is an antimalarial drug, and is sold under the market name Lariam (111). The most interesting part about the drugs, are the adverse effects. Mefloquine is known to cause: seizures, emotional problems, vivid dreams, insomnia, anxiety, depression, basically most of the neuropsychiatric adverse reactions (112). This is of interest, since it seems like the drug may have effect through GABA, and the only way to find out is with more thorough investigation as we can use this information to explain the side-effects seen with Mefloquine.

Rivaroxaban is an anticoagulant used in the treatment of cardiovascular diseases (113). This drug exhibits its effect by directly inhibiting the factor Xa, which is an important factor in the coagulation cascade (114). From the results this compounds seems to have NAM/antagonist activity and it would be interesting to do more testing of this drug. Currently, there is nothing



in the literature that indicates that this drug has an effect on GABA<sub>B</sub> receptor, but a future proposition would be to try a radio ligand binding assay to ensure that the drug actually binds to the receptor. The problem with this approach, is that we currently don't have any radio ligands for our target receptor and it may therefore take some time before any link is mapped out.

The interactions of the hit compounds were investigated and what we can see is that the ligands have the possibility to make strong hydrophobic interaction to the surrounding hydrophobic residues especially Tyr 757 and Trp 752, where pi-pi stacking can be formed.

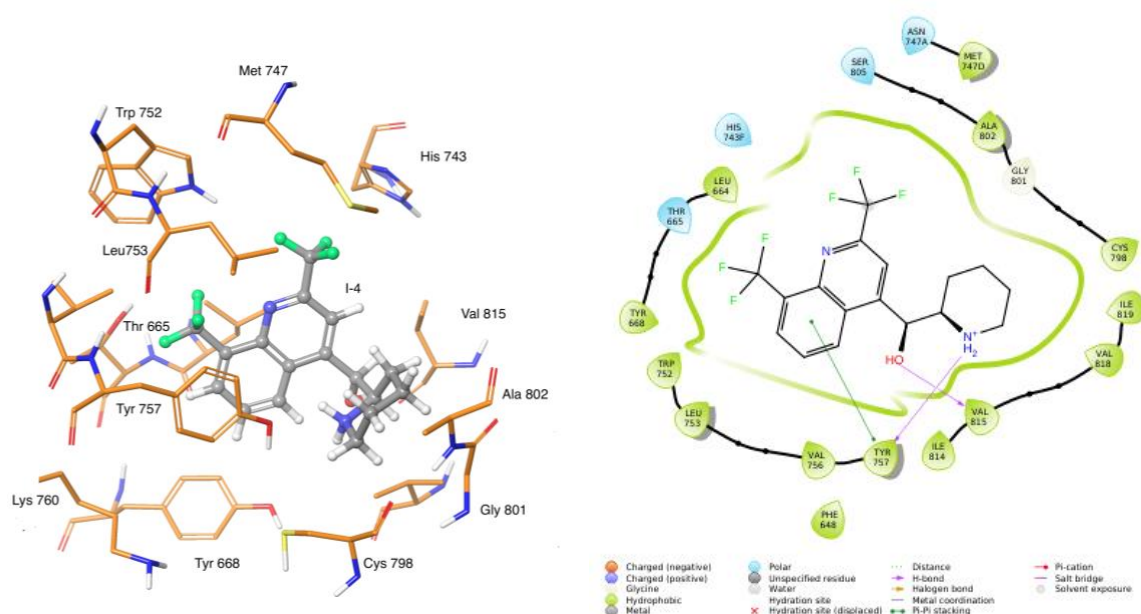


Figure 17 Ligand-receptor complex. A) The figure is a 3D representation that displays the compound I-4 in the binding pocket and the interactions that takes place. B) The figure shows exactly the same, just in 2D. The residues in the picture are 3Å from the ligand.

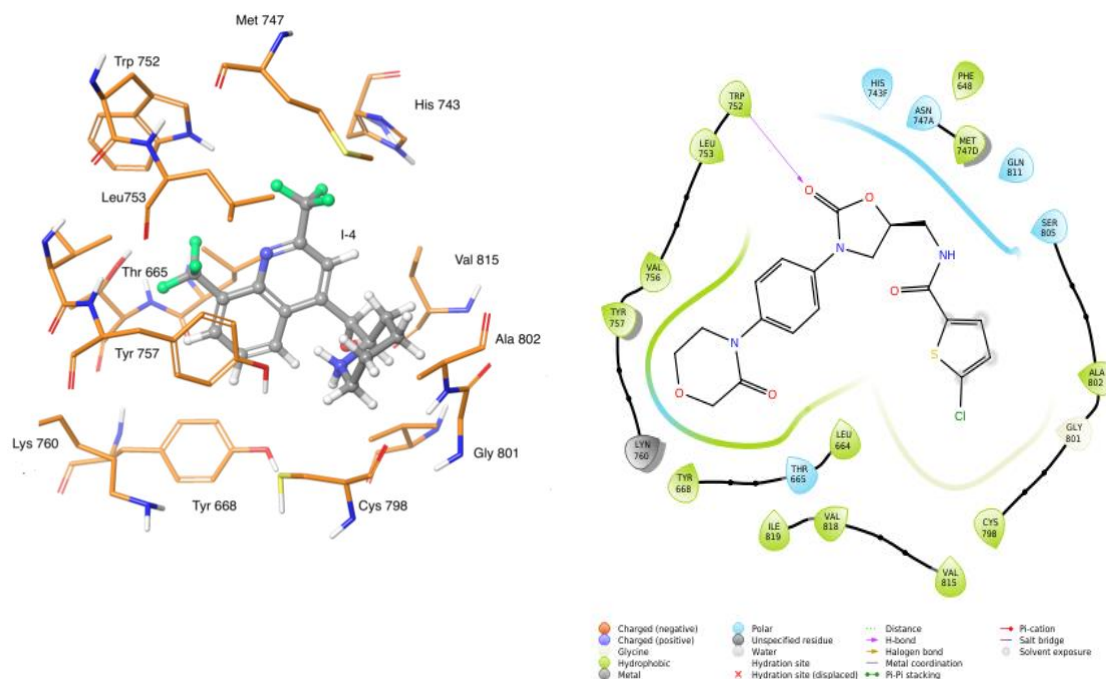


Figure 18 Ligand-receptor complex. A) The figure is a 3D representation that displays the compound I-10 in the binding pocket and the interactions that can take place. B) The figure shows exactly the same, just in 2D. The residues in the picture are 3Å from the ligand.

A comparison with the binding mode of TI-400 shows that many of the same residues are included in the interactions, although the hit compounds is shown to maybe interact with more residues due to their size. However, this gives us an optimistic feeling that the hit compounds may modulate their effect via GABA<sub>B</sub> receptor, although one can never be too sure without doing more experimental tests with the compounds, and wait for the three-dimensional structure of the receptor to finally be solved. That way we'll be able do a more thorough investigation of the binding site, and the binding mode.

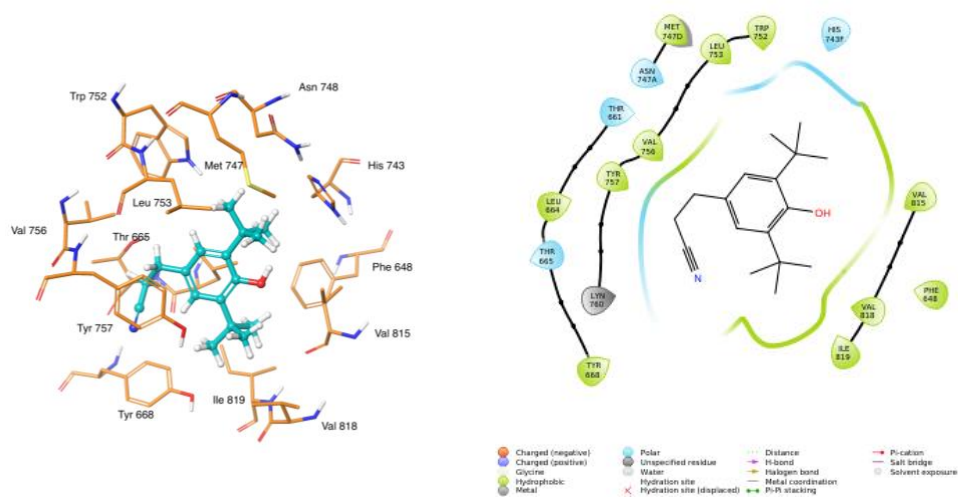


Figure 19 Ligand-receptor complex. A) The top figure is a 3D representation that displays the compound TI-400 in the binding pocket and the interactions that can take place. B) The bottom figure shows exactly the same, just in 2D. The residues in the picture are 3Å from the ligand.

The hits from Molport, I-23 and I-24, seem to exhibit PAM like activity on the receptor. We would like to assume that's the case because of the structure similarity to TI-400, but because of the COVID-19 outbreak earlier this year we weren't able to do enough experimental tests on these compounds. Most of the in vitro testing were done by one of our supervisors Imin Wushur, and because of that we decided to use more time on the compounds from the DrugBank, since they are more diverse than the compounds screened from Molport. Had we had more time, we would've scheduled further testing on the hits as we have high hopes for them being real drug candidates that could be used in the treatment of CNS disorders.

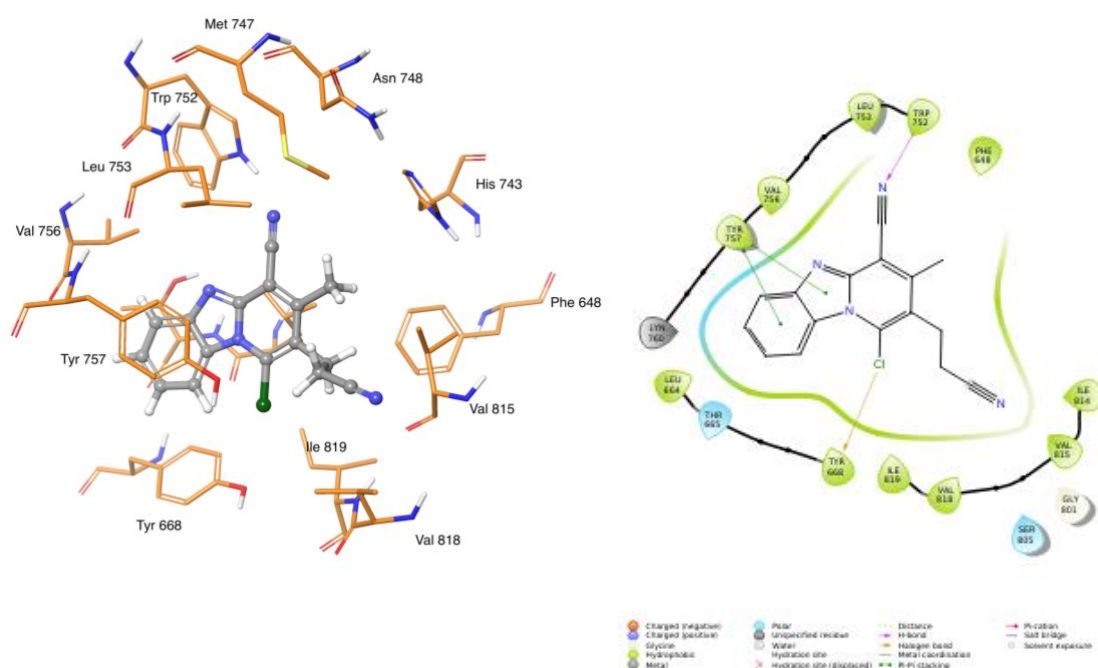


Figure 20 Ligand-receptor complex. A) The figure is a 3D representation that displays the compound I-23 in the binding pocket and the interactions that can take place. B) The figure shows exactly the same, just in 2D. The residues in the picture are 3Å from the ligand.

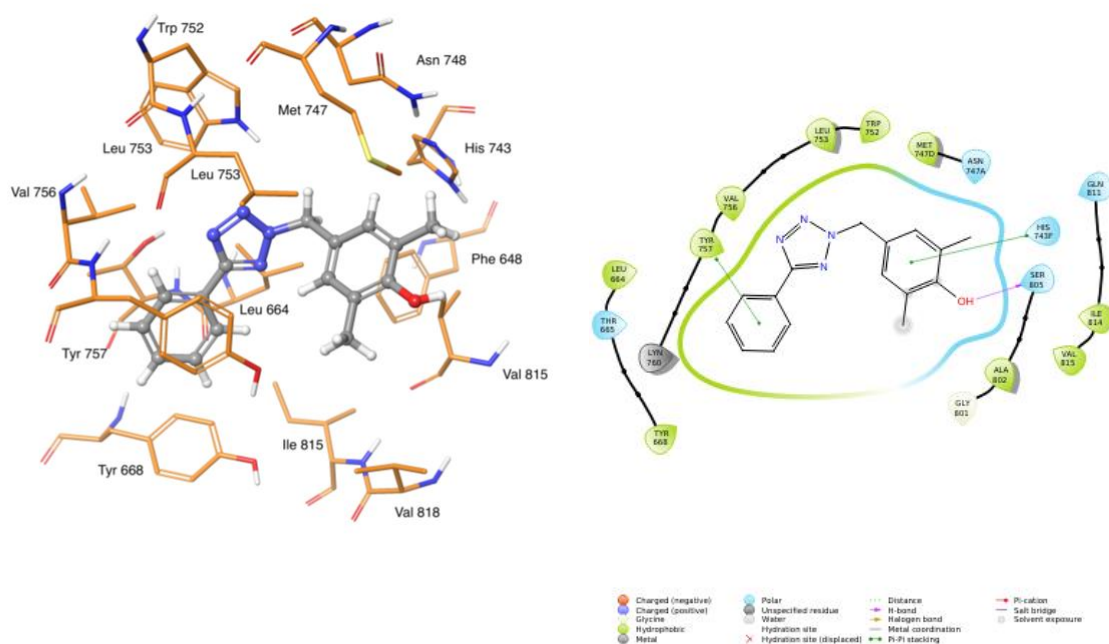


Figure 21 Ligand-receptor complex. A) The figure is a 3D representation that displays the compound I-24 in the binding pocket and the interactions that can take place. B) The figure shows exactly the same, just in 2D. The residues in the picture are 3Å from the ligand.

## 6 Conclusion

In this study we constructed multiple homology models of the GABA<sub>B</sub> receptor, based on an active-like structure of mGlu1. We also used techniques within SBVS and LBVS to screen for new allosteric modulators. Despite the flaws with the techniques and protocols used, we were still able to identify four potential allosteric modulators from both Molport (I-23 and I-24) and the DrugBank (I-4 = Mefloquine and I-10 = Rivaroxaban). The results indicate that I-4 might be a potential PAM and I-10 a NAM/antagonist. I-4 seems to be more of an interest, because of the adverse effects that could be explained through the GABAergic system. Rivaroxaban on the other hand, is a drug with poor bioavailability and may not cross the blood brain barrier. The future solution may be to use this drug as reference for new GABA<sub>B</sub> modulators.

Therefore, its urged to continue to investigate and validate the potential hits, as they may have a key role in the future treatment of CNS disorders.

1. Sherwood L. Human physiology: from cells to systems. 7th ed. Australia ; United States: Brooks/Cole, Cengage Learning; 2010. 1 p.
2. McEwen - 2016 - Central Role of the Brain in Stress and Adaptation.pdf.
3. Torday JS. Homeostasis as the Mechanism of Evolution. *Biology*. 2015 Sep 15;4(3):573–90.
4. Lasakosvitsch F. Introductory Chapter: Homeostasis. *Homeost - Integr Vis* [Internet]. 2018 Nov 5 [cited 2020 Mar 8]; Available from: <https://www.intechopen.com/books/homeostasis-an-integrated-vision/introductory-chapter-homeostasis>
5. Modell H, Cliff W, Michael J, McFarland J, Wenderoth MP, Wright A. A physiologist's view of homeostasis. *Adv Physiol Educ*. 2015 Dec;39(4):259–66.
6. Palaparathi S. Role of Homeostasis in Human Physiology: A Review. *J Med Physiol Ther*. 2017 Apr 12;1(2):1–5.
7. Human Physiology. Blacksleet River; 434 p.
8. Pereda AE. Electrical synapses and their functional interactions with chemical synapses. *Nat Rev Neurosci*. 2014 Apr;15(4):250–63.
9. Zhou Y, Danbolt NC. Glutamate as a neurotransmitter in the healthy brain. *J Neural Transm*. 2014;121(8):799–817.
10. Bartee L, Shriner W, Creech C. Types of Receptors. In: *Principles of Biology: Biology 211, 212, and 213* [Internet]. Open Oregon Educational Resources; 2017 [cited 2020 May 9]. Available from: <https://openoregon.pressbooks.pub/mhccmajorsbio/chapter/types-of-receptors/>
11. Waxham MN. Chapter 10 - Neurotransmitter Receptors. In: Byrne JH, Heidelberger R, Waxham MN, editors. *From Molecules to Networks (Third Edition)* [Internet]. Boston: Academic Press; 2014 [cited 2020 May 9]. p. 285–321. Available from: <http://www.sciencedirect.com/science/article/pii/B9780123971791000105>
12. Kannampalli P, Sengupta JN. Role of Principal Ionotropic and Metabotropic

- Receptors in Visceral Pain. *J Neurogastroenterol Motil.* 2015 Apr 30;21(2):147–58.
13. Rang HP, Dale MM, Ritter JM, Flower RJ, Henderson G. Rang and Dale's pharmacology. Eighth edition. Edinburgh? Elsevier, Churchill Livingstone; 2016. 760 p.
  14. Eisen D, Planatscher H, Hardie DB, Kraushaar U, Pynn CJ, Stoll D, et al. G protein-coupled receptor quantification using peptide group-specific enrichment combined with internal peptide standard reporter calibration. *J Proteomics.* 2013 Sep 2;90:85–95.
  15. Sriram K, Insel PA. G Protein-Coupled Receptors as Targets for Approved Drugs: How Many Targets and How Many Drugs? *Mol Pharmacol.* 2018 Apr;93(4):251–8.
  16. Ban T, Li X, Ma X, Yang H, Song Y, Sun Y, et al. GPCR structure and function relationship: identification of a biased apelin receptor mutant. *Biochem J.* 2018 Dec 12;475(23):3813–26.
  17. Purves D, Augustine GJ, Fitzpatrick D, Katz LC, LaMantia A-S, McNamara JO, et al. Two Families of Postsynaptic Receptors. *Neurosci 2nd Ed [Internet].* 2001 [cited 2020 May 9]; Available from: <https://www.ncbi.nlm.nih.gov/books/NBK10855/>
  18. Kroeze WK, Sheffler DJ, Roth BL. G-protein-coupled receptors at a glance. *J Cell Sci.* 2003 Dec 15;116(24):4867–9.
  19. Fredriksson R, Lagerström MC, Lundin L-G, Schiöth HB. The G-Protein-Coupled Receptors in the Human Genome Form Five Main Families. Phylogenetic Analysis, Paralogon Groups, and Fingerprints. *Mol Pharmacol.* 2003 Jun 1;63(6):1256–72.
  20. Gurevich VV, Gurevich EV. GPCR monomers and oligomers: it takes all kinds. *Trends Neurosci.* 2008 Feb;31(2):74–81.
  21. Wang W, Qiao Y, Li Z. New Insights into Modes of GPCR Activation. *Trends Pharmacol Sci.* 2018 Apr;39(4):367–86.
  22. Wang et al. - 2018 - New Insights into Modes of GPCR Activation.pdf [Internet]. [cited 2020 Mar 22]. Available from: [https://www.cell.com/trends/pharmacological-sciences/pdf/S0165-6147\(18\)30024-5.pdf](https://www.cell.com/trends/pharmacological-sciences/pdf/S0165-6147(18)30024-5.pdf)
  23. Hille B, Dickson E, Kruse M, Falkenburger B. Chapter Ten - Dynamic Metabolic



Control of an Ion Channel. In: Blackwell KT, editor. Progress in Molecular Biology and Translational Science [Internet]. Academic Press; 2014 [cited 2020 May 9]. p. 219–47. (Computational Neuroscience; vol. 123). Available from: <http://www.sciencedirect.com/science/article/pii/B9780123978974000085>

24. Marrari Y, Crouthamel M, Irannejad R, Wedegaertner PB. Assembly and Trafficking of Heterotrimeric G Proteins. *Biochemistry*. 2007 Jul 3;46(26):7665–77.
25. Kobilka BK. G protein coupled receptor structure and activation. *Biochim Biophys Acta BBA - Biomembr*. 2007 Apr 1;1768(4):794–807.
26. Park PS-H, Lodowski DT, Palczewski K. Activation of G Protein–Coupled Receptors: Beyond Two-State Models and Tertiary Conformational Changes. *Annu Rev Pharmacol Toxicol*. 2008;48:107–41.
27. Gassmann M, Bettler B. Regulation of neuronal GABA B receptor functions by subunit composition. *Nat Rev Neurosci*. 2012 Jun;13(6):380–94.
28. Jean-Charles P-Y, Freedman NJ, Shenoy SK. Chapter Nine - Cellular Roles of Beta-Arrestins as Substrates and Adaptors of Ubiquitination and Deubiquitination. In: Shenoy SK, editor. Progress in Molecular Biology and Translational Science [Internet]. Academic Press; 2016 [cited 2020 May 13]. p. 339–69. (Ubiquitination and Transmembrane Signaling; vol. 141). Available from: <http://www.sciencedirect.com/science/article/pii/S1877117316300047>
29. Jean-Charles P-Y, Kaur S, Shenoy SK. GPCR signaling via  $\beta$ -arrestin-dependent mechanisms. *J Cardiovasc Pharmacol*. 2017 Sep;70(3):142–58.
30. Hu G-M, Mai T-L, Chen C-M. Visualizing the GPCR Network: Classification and Evolution. *Sci Rep*. 2017 Nov 14;7(1):1–15.
31. Schiöth HB, Fredriksson R. The GRAFS classification system of G-protein coupled receptors in comparative perspective. *Gen Comp Endocrinol*. 2005 May 15;142(1–2):94–101.
32. McCorvy JD, Roth BL. Structure and Function of Serotonin G protein Coupled Receptors. *Pharmacol Ther*. 2015 Jun;150:129–42.
33. Bertheleme N, Chae PS, Singh S, Mossakowska D, Hann MM, Smith KJ, et al. Unlocking the secrets of the gatekeeper: Methods for stabilizing and crystallizing GPCRs.

Biochim Biophys Acta BBA - Biomembr. 2013 Nov 1;1828(11):2583–91.

34. Chun L, Zhang W, Liu J. Structure and ligand recognition of class C GPCRs. *Acta Pharmacol Sin.* 2012 Mar;33(3):312–23.
35. Foster DJ, Conn PJ. Allosteric modulation of GPCRs: new insights and potential utility for treatment of schizophrenia and other CNS disorders. *Neuron.* 2017 May 3;94(3):431–46.
36. Kenakin TP. Chapter 5 - Allosteric Drug Effects. In: Kenakin TP, editor. *Pharmacology in Drug Discovery and Development (Second Edition)* [Internet]. Academic Press; 2017 [cited 2020 May 10]. p. 101–29. Available from: <http://www.sciencedirect.com/science/article/pii/B9780128037522000053>
37. Woollard SM, Kanmogne GD. Maraviroc: a review of its use in HIV infection and beyond. *Drug Des Devel Ther.* 2015 Oct 1;9:5447–68.
38. Burford NT, Clark MJ, Wehrman TS, Gerritz SW, Banks M, O’Connell J, et al. Discovery of positive allosteric modulators and silent allosteric modulators of the  $\mu$ -opioid receptor. *Proc Natl Acad Sci U S A.* 2013 Jun 25;110(26):10830–5.
39. Wold EA, Zhou J. GPCR Allosteric Modulators: Mechanistic Advantages and Therapeutic Applications. *Curr Top Med Chem.* 2018;18(23):2002–6.
40. Niswender CM, Conn PJ. Metabotropic Glutamate Receptors: Physiology, Pharmacology, and Disease. *Annu Rev Pharmacol Toxicol.* 2010;50:295–322.
41. Papasergi-Scott MM, Robertson MJ, Seven AB, Panova O, Mathiesen JM, Skiniotis G. Structures of metabotropic GABAB receptor. *bioRxiv.* 2020 Apr 16;2020.04.15.004267.
42. Wu H, Wang C, Gregory KJ, Han GW, Cho HP, Xia Y, et al. Structure of a Class C GPCR Metabotropic Glutamate Receptor 1 Bound to an Allosteric Modulator. *Science.* 2014 Apr 4;344(6179):58–64.
43. Levitz J, Habrian C, Bharill S, Fu Z, Vafabakhsh R, Isacoff EY. Mechanism of assembly and cooperativity of homomeric and heteromeric metabotropic glutamate receptors. *Neuron.* 2016 Oct 5;92(1):143–59.

44. Koehl A, Hu H, Feng D, Sun B, Zhang Y, Robertson MJ, et al. Structural insights into the activation of metabotropic glutamate receptors. *Nature*. 2019 Feb;566(7742):79–84.
45. Grushevskiy EO, Kukaj T, Schmauder R, Bock A, Zabel U, Schwabe T, et al. Stepwise activation of a class C GPCR begins with millisecond dimer rearrangement. *Proc Natl Acad Sci U S A*. 2019 May 14;116(20):10150–5.
46. Kniazeff J, Bessis A-S, Maurel D, Ansanay H, Prézeau L, Pin J-P. Closed state of both binding domains of homodimeric mGlu receptors is required for full activity. *Nat Struct Mol Biol*. 2004 Aug;11(8):706–13.
47. Purves D, Augustine GJ, Fitzpatrick D, Katz LC, LaMantia A-S, McNamara JO, et al. GABA and Glycine. *Neurosci 2nd Ed* [Internet]. 2001 [cited 2020 May 11]; Available from: <https://www.ncbi.nlm.nih.gov/books/NBK11084/>
48. Wong CGT, Bottiglieri T, Snead OC. GABA,  $\gamma$ -hydroxybutyric acid, and neurological disease. *Ann Neurol*. 2003;54(S6):S3–12.
49. Olsen RW, Li G-D. Chapter 18 - GABA. In: Brady ST, Siegel GJ, Albers RW, Price DL, editors. *Basic Neurochemistry (Eighth Edition)* [Internet]. New York: Academic Press; 2012 [cited 2020 May 11]. p. 367–76. Available from: <http://www.sciencedirect.com/science/article/pii/B9780123749475000183>
50. Bowery NG, Hill DR, Hudson AL. Characteristics of GABAB receptor binding sites on rat whole brain synaptic membranes. *Br J Pharmacol*. 1983 Jan;78(1):191–206.
51. Frangaj A, Fan QR. Structural biology of GABAB receptor. *Neuropharmacology*. 2018 Jul;136:68–79.
52. Chalifoux JR, Carter AG. GABAB receptor modulation of synaptic function. *Curr Opin Neurobiol*. 2011 Apr;21(2):339–44.
53. Herrick-Davis K, Milligan G, Giovanni GD. *G-Protein-Coupled Receptor Dimers*. Springer; 2017. 502 p.
54. Geng Y, Bush M, Mosyak L, Wang F, Fan QR. Structural mechanism of ligand activation in human GABA B receptor. *Nature*. 2013 Dec;504(7479):254–9.

55. Adams CL, Lawrence AJ. CGP7930: a positive allosteric modulator of the GABAB receptor. *CNS Drug Rev.* 2007;13(3):308–16.
56. Pin J-P, Prézeau L. Allosteric Modulators of GABAB Receptors: Mechanism of Action and Therapeutic Perspective. *Curr Neuropharmacol.* 2007 Oct 1;5:195–201.
57. Sallerin B, Lazorthes Y. [Intrathecal baclofen. Experimental and pharmacokinetic studies]. *Neurochirurgie.* 2003 May;49(2-3 Pt 2):271–5.
58. Wise A, Green A, Main MJ, Wilson R, Fraser N, Marshall FH. Calcium sensing properties of the GABAB receptor. *Neuropharmacology.* 1999 Nov 1;38(11):1647–56.
59. Galvez T, Urwyler S, Prézeau L, Mosbacher J, Joly C, Malitschek B, et al. Ca(2+) requirement for high-affinity gamma-aminobutyric acid (GABA) binding at GABA(B) receptors: involvement of serine 269 of the GABA(B)R1 subunit. *Mol Pharmacol.* 2000 Mar;57(3):419–26.
60. Gasparini F, Spooren W. Allosteric Modulators for mGlu Receptors. *Curr Neuropharmacol.* 2007 Sep;5(3):187–94.
61. Gasparini F, Kuhn R, Pin J-P. Allosteric modulators of group I metabotropic glutamate receptors: novel subtype-selective ligands and therapeutic perspectives. *Curr Opin Pharmacol.* 2002 Feb 1;2(1):43–9.
62. Binet V, Duthey B, Lecaillon J, Vol C, Quoyer J, Labesse G, et al. Common Structural Requirements for Heptahelical Domain Function in Class A and Class C G Protein-coupled Receptors. *J Biol Chem.* 2007 Apr 20;282(16):12154–63.
63. Dupuis DS, Relkovic D, Lhuillier L, Mosbacher J, Kaupmann K. Point Mutations in the Transmembrane Region of GABAB2 Facilitate Activation by the Positive Modulator N,N'-Dicyclopentyl-2-methylsulfanyl-5-nitro-pyrimidine-4,6-diamine (GS39783) in the Absence of the GABAB1 Subunit. *Mol Pharmacol.* 2006 Dec 1;70(6):2027–36.
64. Patrick GL. *An Introduction to Medicinal Chemistry.* Oxford University Press; 2017. 911 p.
65. A P, Lakshmana P S, A U. *Computer Applications in Drug Discovery and Development.* IGI Global; 2018. 348 p.

66. Sousa SF, Ribeiro AJM, Neves RPP, Brás NF, Cerqueira NMFS, Fernandes PA, et al. Application of quantum mechanics/molecular mechanics methods in the study of enzymatic reaction mechanisms. *WIREs Comput Mol Sci*. 2017;7(2):e1281.
67. Scherrer A, Agostini F, Sebastiani D, Gross EKV, Vuilleumier R. On the Mass of Atoms in Molecules: Beyond the Born-Oppenheimer Approximation. *Phys Rev X*. 2017 Aug 25;7(3):031035.
68. Monticelli L, Tieleman DP. Force Fields for Classical Molecular Dynamics. In: Monticelli L, Salonen E, editors. *Biomolecular Simulations* [Internet]. Totowa, NJ: Humana Press; 2013 [cited 2020 Mar 23]. p. 197–213. Available from: [http://link.springer.com/10.1007/978-1-62703-017-5\\_8](http://link.springer.com/10.1007/978-1-62703-017-5_8)
69. Alberts B, Johnson A, Lewis J, Raff M, Roberts K, Walter P. Analyzing Protein Structure and Function. *Mol Biol Cell* 4th Ed [Internet]. 2002 [cited 2020 Mar 23]; Available from: <https://www.ncbi.nlm.nih.gov/books/NBK26820/>
70. Vyas VK, Ukawala RD, Ghate M, Chintha C. Homology Modeling a Fast Tool for Drug Discovery: Current Perspectives. *Indian J Pharm Sci*. 2012;74(1):1–17.
71. Waterhouse A, Bertoni M, Bienert S, Studer G, Tauriello G, Gumienny R, et al. SWISS-MODEL: homology modelling of protein structures and complexes. *Nucleic Acids Res*. 2018 Jul 2;46(Web Server issue):W296–303.
72. *Advances in Protein Chemistry and Structural Biology*. Academic Press; 2014. 484 p.
73. Nayeem A, Sitkoff D, Krystek S. A comparative study of available software for high-accuracy homology modeling: From sequence alignments to structural models. *Protein Sci Publ Protein Soc*. 2006 Apr;15(4):808–24.
74. Ho BK, Brasseur R. The Ramachandran plots of glycine and pre-proline. *BMC Struct Biol*. 2005 Aug 16;5(1):14.
75. Wiltgen M. Algorithms for Structure Comparison and Analysis: Homology Modelling of Proteins. In: Ranganathan S, Gribskov M, Nakai K, Schönbach C, editors. *Encyclopedia of Bioinformatics and Computational Biology* [Internet]. Oxford: Academic Press; 2019 [cited 2020 May 14]. p. 38–61. Available from:

<http://www.sciencedirect.com/science/article/pii/B9780128096338204846>

76. Ramachandran Plot [Internet]. [cited 2020 May 14]. Available from:  
[http://www.cryst.bbk.ac.uk/PPS95/course/3\\_geometry/rama.html](http://www.cryst.bbk.ac.uk/PPS95/course/3_geometry/rama.html)
77. Cheng Y, Glaeser RM, Nogales E. How Cryo-EM Became so Hot. *Cell*. 2017 Nov 30;171(6):1229–31.
78. Gani OA. BSM. Signposts of Docking and Scoring in Drug Design. *Chem Biol Drug Des*. 2007 Oct;70(4):360–5.
79. Wermuth CG. *Glossary Of Terms used in medicinal Chemistry*. Pure and Applied Chemistry; 2009.
80. Fu H. *Chemical Genomics*. Cambridge University Press; 2012. 359 p.
81. Kaserer T, Beck KR, Akram M, Odermatt A, Schuster D. Pharmacophore Models and Pharmacophore-Based Virtual Screening: Concepts and Applications Exemplified on Hydroxysteroid Dehydrogenases. *Molecules*. 2015 Dec 19;20(12):22799–832.
82. Wermuth CG. Pharmacophores: Historical Perspective and Viewpoint from a Medicinal Chemist. In: *Pharmacophores and Pharmacophore Searches* [Internet]. John Wiley & Sons, Ltd; 2006 [cited 2020 Mar 23]. p. 1–13. Available from:  
<https://onlinelibrary.wiley.com/doi/abs/10.1002/3527609164.ch1>
83. Helma C. *Predictive Toxicology*. CRC Press; 2005. 522 p.
84. Peter SC, Dhanjal JK, Malik V, Radhakrishnan N, Jayakanthan M, Sundar D. Quantitative Structure-Activity Relationship (QSAR): Modeling Approaches to Biological Applications. In: *Encyclopedia of Bioinformatics and Computational Biology* [Internet]. Elsevier; 2019 [cited 2020 Mar 23]. p. 661–76. Available from:  
<https://linkinghub.elsevier.com/retrieve/pii/B9780128096338201970>
85. Duan J, Dixon SL, Lowrie JF, Sherman W. Analysis and comparison of 2D fingerprints: Insights into database screening performance using eight fingerprint methods. *J Mol Graph Model*. 2010 Sep;29(2):157–70.
86. Willett P. Similarity Searching Using 2D Structural Fingerprints. In: Bajorath J, editor.

Chemoinformatics and Computational Chemical Biology [Internet]. Totowa, NJ: Humana Press; 2011 [cited 2020 May 12]. p. 133–58. (Methods in Molecular Biology). Available from: [https://doi.org/10.1007/978-1-60761-839-3\\_5](https://doi.org/10.1007/978-1-60761-839-3_5)

87. Langer T, Wolber G. Virtual combinatorial chemistry and in silico screening: Efficient tools for lead structure discovery? *Pure Appl Chem*. 2004 Jan 1;76(5):991–6.

88. Wishart DS, Knox C, Guo AC, Cheng D, Shrivastava S, Tzur D, et al. DrugBank: a knowledgebase for drugs, drug actions and drug targets. *Nucleic Acids Res*. 2008 Jan;36(Database issue):D901–6.

89. Medina-Franco JL, Yoo J, Dueñas-González A. Chapter 13 - DNA Methyltransferase Inhibitors for Cancer Therapy. In: Zheng YG, editor. *Epigenetic Technological Applications* [Internet]. Boston: Academic Press; 2015 [cited 2020 May 12]. p. 265–90. Available from: <http://www.sciencedirect.com/science/article/pii/B9780128010808000132>

90. Astin JW, Keerthisinghe P, Du L, Sanderson LE, Crosier KE, Crosier PS, et al. Chapter 2 - Innate immune cells and bacterial infection in zebrafish. In: Detrich HW, Westerfield M, Zon LI, editors. *Methods in Cell Biology* [Internet]. Academic Press; 2017 [cited 2020 May 12]. p. 31–60. (The Zebrafish; vol. 138). Available from: <http://www.sciencedirect.com/science/article/pii/S0091679X16301388>

91. LigPrep User Manual. :102.

92. Ramírez D, Caballero J. Is It Reliable to Use Common Molecular Docking Methods for Comparing the Binding Affinities of Enantiomer Pairs for Their Protein Target? *Int J Mol Sci* [Internet]. 2016 Apr 20 [cited 2020 May 4];17(4). Available from: <https://www.ncbi.nlm.nih.gov/pmc/articles/PMC4848981/>

93. Friesner RA, Banks JL, Murphy RB, Halgren TA, Klicic JJ, Mainz DT, et al. Glide: A New Approach for Rapid, Accurate Docking and Scoring. 1. Method and Assessment of Docking Accuracy. *J Med Chem*. 2004 Mar;47(7):1739–49.

94. Gabrielsen M, Sylte I, Dahl SG, Ravna AW. A short update on the structure of drug binding sites on neurotransmitter transporters. *BMC Res Notes*. 2011 Dec 22;4:559.

95. Minuesa G, Albanese SK, Xie W, Kazansky Y, Worroll D, Chow A, et al. Small-

molecule targeting of MUSASHI RNA-binding activity in acute myeloid leukemia. *Nat Commun.* 2019 Jun 19;10(1):1–15.

96. Negron C, Pearlman DA, Angel G del. Predicting mutations deleterious to function in beta-lactamase TEM1 using MM-GBSA. *PLOS ONE.* 2019 Mar 19;14(3):e0214015.

97. Freyd T, Warszycki D, Mordalski S, Bojarski AJ, Sylte I, Gabrielsen M. Ligand-guided homology modelling of the GABAB2 subunit of the GABAB receptor. Lodola A, editor. *PLOS ONE.* 2017 Mar 21;12(3):e0173889.

98. Huang N, Shoichet BK, Irwin JJ. Benchmarking Sets for Molecular Docking. *J Med Chem.* 2006 Nov;49(23):6789–801.

99. Czarnik AW, Mei H-Y. 2.12 - How and Why to Apply the Latest Technology\*. In: Taylor JB, Triggle DJ, editors. *Comprehensive Medicinal Chemistry II* [Internet]. Oxford: Elsevier; 2007 [cited 2020 May 14]. p. 289–557. Available from: <http://www.sciencedirect.com/science/article/pii/B008045044X000481>

100. Kenakin TP. Chapter 11 - Pharmacology in Drug Discovery. In: Kenakin TP, editor. *Pharmacology in Drug Discovery and Development (Second Edition)* [Internet]. Academic Press; 2017 [cited 2020 May 14]. p. 275–99. Available from: <http://www.sciencedirect.com/science/article/pii/B9780128037522000119>

101. Lipinski CA, Lombardo F, Dominy BW, Feeney PJ. Experimental and computational approaches to estimate solubility and permeability in drug discovery and development settings. *Adv Drug Deliv Rev.* 2012 Dec 1;64:4–17.

102. Pollastri MP. Overview on the Rule of Five. *Curr Protoc Pharmacol.* 2010;49(1):9.12.1-9.12.8.

103. Veber DF, Johnson SR, Cheng H-Y, Smith BR, Ward KW, Kopple KD. Molecular Properties That Influence the Oral Bioavailability of Drug Candidates. *J Med Chem.* 2002 Jun 1;45(12):2615–23.

104. Keerthy HK, Vivek HK, Bharathkumar H, Rangappa S, Bulusu KC, Mervin LH, et al. MOLPRINT 2D-based identification and synthesis of novel chromene based small molecules that target PLA2: validation through chemo- and bioinformatics approaches. *RSC Adv.* 2015



Oct 20;5(109):89797–808.

105. Jasial S, Hu Y, Vogt M, Bajorath J. Activity-relevant similarity values for fingerprints and implications for similarity searching. *F1000Research* [Internet]. 2016 Apr 28 [cited 2020 May 7];5. Available from: <https://www.ncbi.nlm.nih.gov/pmc/articles/PMC4830209/>

106. QikProp Descriptors and Properties. 2012;3.

107. Sastry M, Lowrie JF, Dixon SL, Sherman W. Large-Scale Systematic Analysis of 2D Fingerprint Methods and Parameters to Improve Virtual Screening Enrichments. *J Chem Inf Model*. 2010 May 24;50(5):771–84.

108. Sessa L, Di Biasi L, Parisi R, Concilio S, Piotto S. Receptor flexibility in molecular cross-docking [Internet]. *PeerJ Preprints*; 2016 Jul [cited 2020 May 13]. Available from: <https://peerj.com/preprints/2199v1>

109. Wong CF. Flexible receptor docking for drug discovery. *Expert Opin Drug Discov*. 2015 Nov 2;10(11):1189–200.

110. Conn PJ, Lindsley CW, Meiler J, Niswender CM. Opportunities and challenges in the discovery of allosteric modulators of GPCRs for treating CNS disorders. *Nat Rev Drug Discov*. 2014 Sep;13(9):692–708.

111. Mefloquine [Internet]. [cited 2020 May 13]. Available from: <https://www.drugbank.ca/drugs/DB00358>

112. Mefloquine Side Effects: Common, Severe, Long Term [Internet]. *Drugs.com*. [cited 2020 May 13]. Available from: <https://www.drugs.com/sfx/mefloquine-side-effects.html>

113. Rivaroxaban [Internet]. [cited 2020 May 13]. Available from: <https://www.drugbank.ca/drugs/DB06228>

114. Cabral KP, Ansell JE. The role of factor Xa inhibitors in venous thromboembolism treatment. *Vasc Health Risk Manag*. 2015 Jan 30;11:117–23.



